

Analysis of scale-dependent kinetic and potential energy in sheared, stably stratified turbulence

Xiaolong Zhang¹, Rohit Dhariwal², Gavin Portwood³,
Stephen M. de Bruyn Kops⁴ and Andrew D. Bragg^{1,†}

¹Department of Civil and Environmental Engineering, Duke University, Durham, NC 27708, USA

²Center for Institutional Research Computing, Washington State University, Pullman, WA 99164, USA

³Lawrence Livermore National Laboratory, Livermore, CA 94550, USA

⁴Department of Mechanical and Industrial Engineering, University of Massachusetts Amherst, Amherst, MA 01003, USA

(Received 19 October 2021; revised 20 June 2022; accepted 20 June 2022)

Budgets of turbulent kinetic energy (TKE) and turbulent potential energy (TPE) at different scales ℓ in sheared, stably stratified turbulence are analysed using a filtering approach. Competing effects in the flow are considered, along with the physical mechanisms governing the energy fluxes between scales, and the budgets are used to analyse data from direct numerical simulation at buoyancy Reynolds number $Re_b = O(100)$. The mean TKE exceeds the TPE by an order of magnitude at the large scales, with the difference reducing as ℓ is decreased. At larger scales, buoyancy is never observed to be positive, with buoyancy always converting TKE to TPE. As ℓ is decreased, the probability of locally convecting regions increases, though it remains small at scales down to the Ozmidov scale. The TKE and TPE fluxes between scales are both downscale on average, and their instantaneous values are correlated positively, but not strongly so, and this occurs due to the different physical mechanisms that govern these fluxes. Moreover, the contributions to these fluxes arising from the sub-grid fields are shown to be significant, in addition to the filtered scale contributions associated with the processes of strain self-amplification, vortex stretching and density gradient amplification. Probability density functions (PDFs) of the Q , R invariants of the filtered velocity gradient are considered and show that as ℓ increases, the sheared-drop shape of the PDF becomes less pronounced and the PDF becomes more symmetric about $R = 0$.

Key words: stratified turbulence

† Email address for correspondence: andrew.bragg@duke.edu

1. Introduction

When turbulence occurs in environmental flows, it is often affected by both mean-shear and stable stratification (Vallis 2006; Ferrari & Wunsch 2009; Wyngaard 2010; Zorzetto, Bragg & Katul 2018; Ayt *et al.* 2020), leading to sheared, stably stratified turbulence (SSST). Mean-shear (vertical gradient of horizontal flow) produces turbulence, with hairpin vortices, streaks and strong fluctuations in all three directions (Lee, Kim & Moin 1990; Pope 2000; Davidson 2004). Stable stratification suppresses fluctuations in the vertical direction, and if sufficiently strong generates a quasi-two-dimensional flow behaviour (Riley & Lelong 2000; Riley & Lindborg 2012). Stable stratification also provides a restoring buoyancy force that enables the propagation of internal waves and the formation of quasi-horizontal ‘pancake’ vortical structures in the flow (Davidson 2004). Since mean-shear and stable stratification have competing effects, and produce different flow structures, the dynamics of SSST are rich and complex. Moreover, the flow is often ‘patchy’, with turbulent and non-turbulent regions interspersed, depending on the local competition between shear and buoyancy. Indeed, when the local shear in the flow is strong enough for the local Richardson number to be sufficiently small, the local flow may undergo Kelvin–Helmholtz instabilities that can evolve due to nonlinearity into turbulent motion (Riley & de Bruyn Kops 2003).

Understanding and modelling SSST is an active area of research with many open questions. One such issue concerns understanding the mixing efficiencies in SSST and their parametric dependence (Peltier & Caulfield 2003; Portwood, de Bruyn Kops & Caulfield 2019), which are vital for predicting mixing in oceans (Jayne 2009; Gregg *et al.* 2018). Another vital area is to understand the properties of SSST across its range of dynamical scales, and the physical mechanisms that govern the fluxes of turbulent kinetic and potential energy between scales. Not only is this important for a basic understanding of the flow, it is also of crucial importance for developing large-eddy simulation (LES) models for SSST. A number of studies have considered the effect of stable stratification on the multiscale properties of turbulence using Fourier analysis and considering the average behaviour of the flow in terms of the energy spectrum, the mean buoyancy and mean interscale energy transfer terms (Riley & de Bruyn Kops 2003; Lindborg 2006; Almkie & de Bruyn Kops 2012). The study of Riley & de Bruyn Kops (2003) showed that the horizontal energy spectrum exhibits a $k_h^{-5/3}$ scaling for wavenumbers smaller than the Ozmidov wavenumber k_O (corresponding to the wavenumber at which inertial and buoyancy forces are of the same order), where k_h is the horizontal wavenumber, and the results indicated a downscale energy transfer of kinetic energy in the flow. This motivated (Lindborg 2006), who confirmed that strongly stratified turbulent flows exhibit a downscale cascade of turbulent kinetic and potential energy on average, and developed phenomenological predictions similar in spirit to Kolmogorov’s 1941 theory (Kolmogorov 1941). The observation of a downscale energy cascade was contrary to predictions that had been made by Gage (1979) and Lilly (1983) based on the assumption that in the limit of strong stratification, the flow should behave as two-dimensional turbulence. The basic reason why the predictions of Gage (1979) and Lilly (1983) failed is that, as shown in Billant & Chomaz (2001), as the strength of the stratification increases and the vertical velocity of the flow is suppressed, the vertical length scale of the flow also reduces in such a way that the terms in the dynamical equations associated with vertical motion always remain $O(1)$, hence the flow never becomes two-dimensional.

Many questions remain, however, regarding the multiscale properties of SSST. For example, how do fluctuations of the SSST flow about its mean-field state behave? What are the mechanisms of the turbulent kinetic and potential energy transfers among

scales, and to what extent are these transfers coupled to each other, and to fluctuations in the local buoyancy? How do the sub-grid scale terms in SSST contribute to the flow dynamics across scales? To address these and other questions, in this paper we will use a filtering-based approach (Liu, Meneveau & Katz 1994; Eyink 1995*a,b*; Meneveau & Katz 2000) wherein the velocity and density fields are considered for different filtering lengths ℓ . The filtering-based approach has been applied previously to the study of energy and potential enstrophy cascades in the context of rotating, stratified flows (Aluie & Kurien 2011). We apply the filtering approach to explore the turbulent kinetic and potential energies at different scales of SSST, and the various processes that determine their behaviour. Using a filtering approach allows us to consider spatially local couplings between the processes that control the flow energetics at different scales, and to consider fluctuations in the flow as well as the mean-field behaviour. Moreover, such an analysis of the multiscale properties of SSST can provide insights for developing LES models of SSST, since LES models are often developed in the physical space, rather than Fourier space, context. LES modelling of stratified turbulence is an underdeveloped area (Khani & Waite 2015), and new insights into the dynamics of stratified turbulence across scales could aid in the development of appropriate sub-grid models.

The outline of the paper is as follows. In § 2, we introduce the equations governing the turbulent kinetic and potential energy at different scales, consider the behaviour of the mean-field state of the flow at different scales, and discuss the physical mechanisms governing the energy transfer among scales in SSST. In § 3, we describe the direct numerical simulations (DNS) dataset used in this study, and in § 4, we present and discuss results from the DNS for the quantities introduced in § 2 that govern the turbulent kinetic and potential energy at different scales. Finally, in § 5, we draw conclusions from the study and discuss areas for future investigation.

2. Theoretical considerations

2.1. Governing equations for scale-dependent energy fields

We consider the case where the mean velocity gradient γ and the mean density gradient ζ (note that $\zeta < 0$) are constant in space and time, such that the total fluid velocity vector can be written as $\mathbf{U} = z\gamma\mathbf{e}_x + \mathbf{u}$, where \mathbf{u} is the fluctuating component of the velocity, and the total density can be written as $\rho = \rho_r + z\zeta + \rho'$, where ρ_r is a constant reference density, and ρ' is the fluctuating component of the density. While \mathbf{e}_x is the unit vector in the direction of the mean velocity ($\langle \mathbf{U} \rangle = z\gamma\mathbf{e}_x$), \mathbf{e}_z is the unit vector pointing in the direction opposite to the gravitational acceleration \mathbf{g} (i.e. the vertical direction), and $\mathbf{e}_y \equiv \mathbf{e}_z \times \mathbf{e}_x$.

The filtering operator to be used is defined for an arbitrary field $\mathbf{a}(\mathbf{x}, t)$ as $\tilde{\mathbf{a}}(\mathbf{x}, t) \equiv \int_{\mathbb{R}^3} \mathbf{a}(\mathbf{x} - \mathbf{y}, t) \mathcal{G}_\ell(\mathbf{y}) d\mathbf{y}$, where \mathcal{G}_ℓ is an isotropic filtering kernel with length scale ℓ . In order for the energy fields introduced below to be strictly non-negative, which is a physical requirement, a necessary and sufficient condition is that the filtering kernel \mathcal{G}_ℓ be non-negative (Vreman, Geurts & Kuerten 1994). We will use the isotropic Gaussian filter $\mathcal{G}_\ell(\mathbf{y}) \equiv (2\pi\ell^2)^{-3/2} \exp(-\|\mathbf{y}\|^2/2\ell^2)$, which satisfies this condition. Further considerations regarding the implications of using different filtering kernels can be found in Sadek & Aluie (2018).

Assuming that $|\rho'|/\rho \ll 1$, the governing equation for \mathbf{u} is then the Boussinesq–Navier–Stokes equation coupled with an advection–diffusion equation for ρ' (Vallis 2006).

The filtered versions of these equations are

$$D_t \tilde{\mathbf{u}} = -(1/\rho_r) \nabla \tilde{p} - \nabla \cdot \boldsymbol{\tau} + 2\nu \nabla \cdot \tilde{\mathbf{s}} - N\tilde{\phi} \mathbf{e}_z + \tilde{\mathbf{F}}, \quad (2.1)$$

$$D_t \tilde{\phi} = -\nabla \cdot \boldsymbol{\Sigma} + \kappa \nabla^2 \tilde{\phi} + N\tilde{u}_z + \tilde{f}, \quad (2.2)$$

where $D_t \equiv \partial_t + \tilde{\mathbf{u}} \cdot \nabla$, $\tilde{\phi} \equiv g\rho'/N\rho_r$ is the scaled density field (with dimensions of a velocity), $g \equiv \|\mathbf{g}\|$, ν and κ are the kinematic viscosity and thermal diffusivity, respectively, $N \equiv \sqrt{-g\zeta/\rho_r}$ is the buoyancy frequency, $\boldsymbol{\tau} \equiv \widetilde{\mathbf{u}\mathbf{u}} - \tilde{\mathbf{u}}\tilde{\mathbf{u}}$ is the sub-grid stress tensor, $\tilde{\mathbf{s}} \equiv (\nabla \tilde{\mathbf{u}} + [\nabla \tilde{\mathbf{u}}]^T)/2$ is the filtered strain rate, and $\boldsymbol{\Sigma} \equiv \widetilde{\mathbf{u}\phi} - \tilde{\mathbf{u}}\tilde{\phi}$ is the sub-grid vector for the scaled density field. The terms \mathbf{F} and f , whose filtered forms appear in the equations above, are the forcing terms associated with mean velocity gradient applied to the flow, and for the SSST under consideration are given by

$$\mathbf{F} = -\gamma(\mathbf{e}_z \cdot \mathbf{x})(\mathbf{e}_x \cdot \nabla)\mathbf{u} - \gamma\mathbf{e}_x(\mathbf{e}_z \cdot \mathbf{u}), \quad (2.3)$$

$$f = -\gamma(\mathbf{e}_z \cdot \mathbf{x})(\mathbf{e}_x \cdot \nabla)\phi. \quad (2.4)$$

Following Germano (1992), the turbulent kinetic energy (TKE) in a given region of size ℓ is $\widetilde{\mathbf{u} \cdot \mathbf{u}}/2$, and this may be split up into the TKE at scales $\geq \ell$ ('large scales') denoted by $E_K \equiv \|\widetilde{\mathbf{u}}\|^2/2$, and the TKE at scales $< \ell$ ('small scales') denoted by $e_K \equiv (\|\mathbf{u}\|^2 - \|\widetilde{\mathbf{u}}\|^2)/2 = \text{tr}[\boldsymbol{\tau}]/2$. The equations governing E_K and e_K may be derived from (2.1) and are given by

$$D_t E_K = -(1/\rho_r) \nabla \cdot (\tilde{\mathbf{u}}\tilde{p}) - \nabla \cdot (\tilde{\mathbf{u}} \cdot \boldsymbol{\tau}) - \Pi_K + 2\nu \nabla \cdot (\tilde{\mathbf{u}} \cdot \tilde{\mathbf{s}}) - 2\nu \|\tilde{\mathbf{s}}\|^2 - N\tilde{u}_z\tilde{\phi} + \tilde{\mathbf{F}} \cdot \tilde{\mathbf{u}}, \quad (2.5)$$

$$D_t e_K = \nabla \cdot \mathbf{T}_K + \mathcal{B} + \Pi_K - \varepsilon_K + \mathcal{F}_K. \quad (2.6)$$

In these equations, the scale-to-scale TKE flux is defined as $\Pi_K \equiv -\boldsymbol{\tau} : \tilde{\mathbf{s}}$, such that $\Pi_K > 0$ corresponds to a transfer of TKE from the large to the small scales. The small-scale buoyancy term is $\mathcal{B} \equiv -N(\widetilde{u_z\phi} - \tilde{u}_z\tilde{\phi})$, the small-scale TKE dissipation rate is $\varepsilon_K \equiv 2\nu(\|\tilde{\mathbf{s}}\|^2 - \|\mathbf{s}\|^2)$, the small-scale forcing is $\mathcal{F}_K \equiv \widetilde{\mathbf{F} \cdot \mathbf{u}} - \tilde{\mathbf{F}} \cdot \tilde{\mathbf{u}}$, and the small-scale TKE transport term involves

$$\mathbf{T}_K \equiv -(1/\rho_r)(\widetilde{\mathbf{u}}\tilde{p} - \tilde{\mathbf{u}}\tilde{p}) - (1/2)(\widetilde{\mathbf{u}\|\mathbf{u}\|^2} - \tilde{\mathbf{u}}\|\tilde{\mathbf{u}}\|^2) + (\tilde{\mathbf{u}} \cdot \boldsymbol{\tau}) + 2\nu(\widetilde{\mathbf{u} \cdot \mathbf{s}} - \tilde{\mathbf{u}} \cdot \tilde{\mathbf{s}}). \quad (2.7)$$

The turbulent potential energy (TPE) in a given region of size ℓ is $\widetilde{\phi\phi}/2$, and this may be split up into the amount contained in the large scales denoted by $E_P \equiv \tilde{\phi}\tilde{\phi}/2$, and the amount contained in the small scales denoted by $e_P \equiv (\phi\phi - \tilde{\phi}\tilde{\phi})/2$. The equations governing E_P and e_P may be derived from (2.2) and are given by

$$D_t E_P = -\nabla \cdot (\tilde{\phi}\boldsymbol{\Sigma}) - \Pi_P + \frac{1}{2}\kappa \nabla^2 \tilde{\phi}\tilde{\phi} - \kappa \|\nabla \tilde{\phi}\|^2 + N\tilde{\phi}\tilde{u}_z + \tilde{\phi}\tilde{f}, \quad (2.8)$$

$$D_t e_P = \nabla \cdot \mathbf{T}_P - \varepsilon_P - \mathcal{B} + \Pi_P + \mathcal{F}_P. \quad (2.9)$$

In these equations, the scale-to-scale TPE flux is defined as $\Pi_P \equiv -\boldsymbol{\Sigma} \cdot \nabla \tilde{\phi}$, such that $\Pi_P > 0$ corresponds to a transfer of TPE from the large to the small scales. The small-scale TPE dissipation rate is $\varepsilon_P \equiv \kappa(\|\nabla \phi\|^2 - \|\nabla \tilde{\phi}\|^2)$, the small-scale scalar forcing is $\mathcal{F}_P \equiv \widetilde{\phi f} - \tilde{\phi}\tilde{f}$, and the small-scale scalar transport involves

$$\mathbf{T}_P \equiv (\kappa/2) \nabla (\tilde{\phi}\phi - \tilde{\phi}\tilde{\phi}) + \tilde{\phi}\boldsymbol{\Sigma}. \quad (2.10)$$

The equations for E_K and E_P shown above ((2.5) and (2.8)) were also derived in the previous study of Aluie & Kurien (2011).

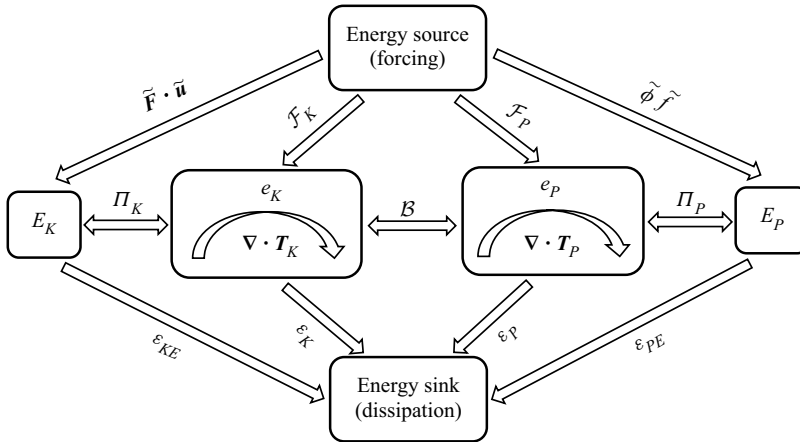


Figure 1. Schematic to illustrate the various energy pathways in the flow. The large-scale TKE field gains energy from the forcing $\tilde{F} \cdot \tilde{u}$, and loses TKE irreversibly through the large-scale TKE dissipation-rate term ε_{KE} . The large-scale TPE field gains energy from the forcing $\tilde{\phi} \tilde{f}$, and loses TPE irreversibly through the large-scale TPE dissipation-rate term ε_{PE} . The small-scale TKE field gains energy from the forcing term \mathcal{F}_K , can lose/gain energy reversibly to/from the large-scale TKE field E_K through the interscale TKE flux term Π_K , can lose/gain energy reversibly to/from the small-scale TPE field e_P through the buoyancy term \mathcal{B} , and loses TKE irreversibly through the TKE dissipation-rate term ε_K . The transport term $\nabla \cdot \mathbf{T}_K$ moves e_K conservatively around in space and so is neither a source nor a sink for e_K . The small-scale TPE field gains energy from the forcing term \mathcal{F}_P , can lose/gain energy reversibly to/from the large-scale TPE field E_P through the interscale TPE flux term Π_P , can lose/gain energy reversibly to/from the small-scale TKE field e_K through the buoyancy term \mathcal{B} , and loses TPE irreversibly through the TPE dissipation-rate term ε_P . The transport term $\nabla \cdot \mathbf{T}_P$ moves e_P conservatively around in space and so is neither a source nor a sink for e_P .

In the following, attention will be given to the behaviour of the terms that contribute to $D_t e_K$ and $D_t e_P$. Note that while e_K and e_P are referred to as the small-scale TKE and TPE, respectively, they correspond to the TKE and TPE contained in all scales $< \ell$, so that when ℓ exceeds the integral length scale of the flow, e_K and e_P actually contain the contributions from the largest dynamical scales in the flow. Furthermore, while we choose to focus on the small-scale fields, the questions that we are interested in exploring can also be addressed from a different vantage point by considering the dynamics of the large-scale fields.

A schematic is shown in figure 1 to illustrate the various energy pathways in the flow according to the equations presented above.

2.2. Length scales in SSST

As discussed in Portwood *et al.* (2019), for the velocity field there are four important length scales for the SSST flow under consideration. The first is the large-eddy length scale, which may be characterized by $L = \mathcal{E}_K^{3/2} / \langle \varepsilon_K \rangle$, where the angle brackets $\langle \rangle$ denote an ensemble average and $\mathcal{E}_K \equiv \lim_{\ell \rightarrow \infty} \langle e_K \rangle$ is the total (i.e. involving contributions from all scales) mean TKE in the flow, and $\langle \varepsilon_K \rangle \equiv \lim_{\ell \rightarrow \infty} \langle \varepsilon_K \rangle$ is the total mean TKE dissipation rate (note that here we are assuming an unbounded flow that is suitable for the SSST under consideration). The second length scale is the Kolmogorov length scale $\eta = (v^3 / \langle \varepsilon_K \rangle)^{1/4}$, which characterizes the scale at which viscous and inertial scales in the flow are of the same order. The third is the Ozmidov length scale $\ell_O = (\langle \varepsilon_K \rangle / N^3)^{1/2}$, which characterizes the scale at which buoyancy and inertial forces are of the same order.

The fourth is the Corrsin length scale $\ell_C = (\langle \epsilon_K \rangle / \gamma^3)^{1/2}$, which characterizes the scale at which mean-shear and inertial forces are of the same order. Different non-dimensional flow parameters may be related to these length scales (assuming $\nu = \kappa$):

$$Ri \equiv \frac{N^2}{\gamma^2} = (\ell_C / \ell_O)^{4/3}, \tag{2.11}$$

$$Fr \equiv \frac{\langle \epsilon_K \rangle}{N \mathcal{E}_K} = (\ell_O / L)^{2/3}, \tag{2.12}$$

$$Re_b \equiv \frac{\langle \epsilon_K \rangle}{\nu N^2} = (\ell_O / \eta)^{4/3}, \tag{2.13}$$

$$Re_s \equiv \frac{\langle \epsilon_K \rangle}{\nu \gamma^2} = (\ell_C / \eta)^{4/3}. \tag{2.14}$$

In order for the flow to become turbulent, the Richardson number must satisfy $Ri < O(1)$ (and therefore $\ell_C < O(\ell_O)$), and in order for stratification to have an impact on the flow, the Froude number must satisfy $Fr < O(1)$. In order for there to exist a range of scales $\ell \ll \ell_O$ that are not affected by buoyancy, the buoyancy Reynolds number must satisfy $Re_b \gg 1$. Correspondingly, in order for there to exist a range of scales $\ell \ll \ell_C$ that are not affected by the mean-shear, the shear Reynolds number must satisfy $Re_s \gg 1$. These Reynolds numbers are, however, related, since $Re_s = Re_b Ri$.

For the scalar field, the large scale is $L_P \equiv \mathcal{E}_P^{3/2} \langle \epsilon_K \rangle^{1/2} / \langle \epsilon_P \rangle^{3/2}$, where $\mathcal{E}_P \equiv \lim_{\ell \rightarrow \infty} \langle e_P \rangle$ is the total mean TPE in the flow, and $\langle \epsilon_P \rangle \equiv \lim_{\ell \rightarrow \infty} \langle \epsilon_P \rangle$ is the total mean TPE dissipation rate. The small scale is the Batchelor scale $\eta_B \equiv (\nu \kappa^2 / \langle \epsilon_K \rangle)^{1/4}$. In this paper, we focus on flows with $\nu = \kappa$ such that $\eta_B = \eta$.

2.3. Mean-field behaviour

We now turn to consider the contributions to the equations governing the mean energy fields $\langle e_K \rangle$ and $\langle e_P \rangle$. For SSST, the mean transport equations for these quantities reduce to

$$0 = \langle \mathcal{B} \rangle - \langle \epsilon_K \rangle + \langle \Pi_K \rangle + \langle \mathcal{F}_K \rangle, \tag{2.15}$$

$$0 = -\langle \mathcal{B} \rangle - \langle \epsilon_P \rangle + \langle \Pi_P \rangle. \tag{2.16}$$

In the following discussion, we will first consider the case where the forcing is confined to the large scales (such as in Lindborg 2006), a flow that we refer to here as forced stably stratified turbulence (FSST), for which we introduce the scale ℓ_F as the scale below which the forcing plays a sub-leading role in the flow (note that $\ell_F \leq O(L)$). This behaviour will then be compared to that of SSST to understand the differences.

Focusing first on the TKE, in the limit $\ell/L \rightarrow \infty$, $\langle \Pi_K \rangle \rightarrow 0$, $\langle \epsilon_K \rangle \rightarrow \langle \epsilon_K \rangle$, $\langle \mathcal{F}_K \rangle \rightarrow \langle \mathcal{F}_K \rangle^\infty$, $\langle \mathcal{B} \rangle \rightarrow \langle \mathcal{B} \rangle^\infty$, so that we have

$$\langle \mathcal{F}_K \rangle^\infty \sim -\langle \mathcal{B} \rangle^\infty + \langle \epsilon_K \rangle, \tag{2.17}$$

reflecting a balance between the total injection of TKE by the forcing and the total energy lost due to viscous dissipation and conversion to TPE. The behaviour of (2.15) and (2.16) as the scale ℓ decreases depends on the dynamical scales of the system that were introduced in § 2.2.

For FSST, $\langle \Pi_K \rangle \sim -\langle \mathcal{B} \rangle + \langle \epsilon_K \rangle$ when $\ell_F \gg \ell \gg \eta$, and for $\ell_O / \ell_F \rightarrow \infty$ (neutrally buoyant), this would correspond to a TKE cascade $\langle \Pi_K \rangle \sim \langle \epsilon_K \rangle$. However, for a stably

stratified flow where $\langle \mathcal{B} \rangle^\infty < 0$, since buoyancy effects reduce with decreasing scale, $\langle \Pi_K \rangle \sim -\langle \mathcal{B} \rangle + \langle \epsilon_K \rangle$ implies that the TKE flux $\langle \Pi_K \rangle$ will actually reduce as ℓ decreases, until it approaches a constant value in the regime $\ell_O > \ell \gg \eta$, as discussed in Riley & Lindborg (2012) and Kumar, Chatterjee & Verma (2014). As a result of this, at scales where buoyancy is active (i.e. $\ell \geq \ell_O$), the TKE flux in stratified turbulence cannot be in the form of a cascade (which would require a constant energy flux). This is simply a reflection of the fact that at these scales, TKE is being lost as it is passed down to smaller scales due to conversion of TKE to TPE.

For SSST, the behaviour of $\langle \Pi_K \rangle$ is quite different. In this case, $\langle \mathcal{F}_K \rangle$ operates down to the scale ℓ_C , so because $\ell_C < \ell_O$, the behaviour $\langle \Pi_K \rangle \sim -\langle \mathcal{B} \rangle + \langle \epsilon_K \rangle$ never emerges, and the regime that emerges instead for $Ri \ll 1$ is $\langle \Pi_K \rangle \sim -\langle \mathcal{F}_K \rangle + \langle \epsilon_K \rangle$ for $\ell \gg \eta$. In this regime, the TKE flux is again not in the form of a cascade since $\langle \mathcal{F}_K \rangle$ depends on ℓ . Indeed, based on the behaviour of the co-spectrum (Katul *et al.* 2013), we might expect the following behaviour to emerge at high Re in SSST:

$$\langle \Pi_K \rangle \sim -\gamma^2 \langle \epsilon_K \rangle^{1/3} \ell^{4/3} + \langle \epsilon_K \rangle, \quad \text{for } L \gg \ell \gg \eta. \quad (2.18)$$

Therefore, in this range $\langle \Pi_K \rangle$ increases as ℓ decreases, until it asymptotes to the constant flux cascade regime $\langle \Pi_K \rangle \sim \langle \epsilon_K \rangle$ for $\ell_C \gg \ell \gg \eta$. This is the opposite behaviour to that discussed in Kumar *et al.* (2014) for FSST, where the forcing is confined to scales $\gg \ell_O$ and where $\langle \Pi_K \rangle$ reduces as ℓ decreases towards ℓ_O .

In the above discussion, it has been assumed that $\langle \epsilon_K \rangle \sim \langle \epsilon_K \rangle$ for $\ell \gg \eta$. While this is true for isotropic turbulence, it will not apply in general in strongly stratified flows with $Fr \ll 1$. This is because when $Fr \ll 1$, the flow structures are highly anisotropic, so while the horizontal length scale may be large enough for viscous effects to be negligible, the vertical length scale of the structure may be small enough for viscous effects to be important (Riley & Lindborg 2012). In such a situation, even if $\langle \Pi_K \rangle \sim \langle \epsilon_K \rangle$ emerges in some range of scales, this would not correspond to an inertial cascade since $\langle \epsilon_K \rangle$ would depend on ℓ .

Concerning the TPE field, for flows with $\nu = \kappa$, we have for $\ell \gg \eta$ that

$$\langle \Pi_P \rangle \sim \langle \mathcal{B} \rangle + \langle \epsilon_P \rangle. \quad (2.19)$$

Hence in the regime $\ell > \ell_O$, as ℓ decreases, $\langle \Pi_P \rangle$ increases, while for $\ell_O \gg \ell \gg \eta$, the constant flux cascade regime $\langle \Pi_P \rangle \sim \langle \epsilon_P \rangle$ emerges. Therefore, there cannot be a TPE cascade in the strict sense at scales where density is an active scalar, i.e. $\ell > \ell_O$, since the scale dependency of $\langle \mathcal{B} \rangle$ at these scales leads to a non-constant flux of TPE at these scales. This observation seems to be in conflict with the well-known Bolgiano–Obukhov (BO) scaling (Bolgiano 1959; Obukhov 1959) that has been proposed for stratified turbulent flows, in which $\langle \Pi_K \rangle$ is supposed to decay with reducing ℓ due to buoyancy as $\langle \Pi_K \rangle \propto \ell^{4/5}$ while $\langle \Pi_P \rangle$ is constant, $\langle \Pi_P \rangle \sim \langle \epsilon_P \rangle$. This behaviour, however, seems problematic. For example, in FSST, for $\ell_F \gg \ell \gg \eta$,

$$\langle \Pi_K \rangle \sim -\langle \mathcal{B} \rangle + \langle \epsilon_K \rangle, \quad (2.20)$$

$$\langle \Pi_P \rangle \sim \langle \mathcal{B} \rangle + \langle \epsilon_P \rangle. \quad (2.21)$$

It would seem that BO scaling could emerge only if $\langle \epsilon_P \rangle \gg \langle \epsilon_K \rangle = O(|\langle \mathcal{B} \rangle|)$, as noted in Alam, Guha & Verma (2019), so that we could have $\langle \Pi_K \rangle \sim -\langle \mathcal{B} \rangle + \langle \epsilon_K \rangle$ in which $\langle \Pi_K \rangle$ reduces as ℓ reduces while $\langle \Pi_P \rangle \sim \langle \epsilon_P \rangle$. However, DNS of FSST show $\langle \epsilon_P \rangle \lesssim \langle \epsilon_K \rangle$ over a range of Fr and Re_b (Lindborg 2006; de Bruyn Kops 2015) that includes the ‘moderately stratified’ regime $Re \gg 1$ and $Fr \approx 1$, for which it has been argued that BO should apply

(Alam *et al.* 2019). In SSST, BO scaling cannot emerge because there are by definition no scales at which the dynamics are given by a balance between inertia and buoyancy forces, since the mean-shear production is larger than the buoyancy at all scales at which it is active, reflected in that SSST requires $\ell_C < \ell_O$.

2.4. Mechanisms governing the TKE and TPE fluxes

Since stable stratification acts to two-dimensionalize the flow, it had been conjectured that such flows might feature an inverse energy cascade (Gage 1979; Lilly 1983). However, it has now been demonstrated that this does not occur, but that there is a forward/downscale cascade of both kinetic and potential energy (Riley & de Bruyn Kops 2003; Lindborg 2005, 2006; Waite & Bartello 2006; Brethouwer *et al.* 2007; Aluie & Kurien 2011). The TKE cascade in homogeneous, isotropic turbulence (HIT) is also downscale on average in three dimensions; however, the underlying mechanisms driving the energy transfers in HIT and SSST might be quite different. In the context of HIT, it has long been thought that the key mechanism driving the TKE cascade is that of vortex stretching (VS) (Taylor 1922, 1938; Tennekes & Lumley 1972; Davidson 2004; Doan *et al.* 2018). However, recent studies have demonstrated quantitatively that while VS plays an important role, the largest contribution to the TKE cascade comes from the dynamical process of the self-amplification of the strain-rate field (Carbone & Bragg 2020; Johnson 2020, 2021). An important question is how this understanding applies to SSST, where effects such as internal waves and mean-shear can play a role (whether directly or indirectly) in how TKE is transferred between scales, as well as the question of the mechanism driving the TPE transfer.

In Johnson (2020, 2021), a powerful, exact relationship was derived for Π_K that assumes only that the filtering kernel \mathcal{G}_ℓ used in constructing $\tilde{\mathbf{u}}$ is Gaussian. The result is

$$\Pi_K = \Pi_K^{F,SSA} + \Pi_K^{F,VS} + \Pi_K^{SG,SSA} + \Pi_K^{SG,VS} + \Pi_K^{SG,C}, \quad (2.22)$$

$$\Pi_K^{F,SSA} = -\ell^2 \tilde{\mathbf{s}} : (\tilde{\mathbf{s}} \cdot \tilde{\mathbf{s}}), \quad (2.23)$$

$$\Pi_K^{F,VS} = (1/4)\ell^2 \tilde{\mathbf{s}} : (\tilde{\boldsymbol{\omega}}\tilde{\boldsymbol{\omega}}), \quad (2.24)$$

where superscript F denotes that the quantity depends on only the filtered fields, while superscript SG denotes that the quantity depends on the sub-grid fields as well as the filtered fields. Explicit integral formulae for the SG terms can be found in Johnson (2020, 2021); we do not quote them here as they will not be considered in detail in the present paper. Note that in Johnson (2020, 2021), the F contributions are referred to as the ‘local’ contributions, while the SG contributions are referred to as ‘non-local’ contributions. While the use of this terminology is appropriate in studies of turbulence (L’vov & Falkovich 1992; Eyink 2005; Aluie & Eyink 2009), we prefer to avoid it, because typically in turbulence, a local energy flux is taken to imply an energy flux dominated by the interaction between scales of similar size, which is not necessarily a property possessed by $\Pi_K^{F,SSA}$ and $\Pi_K^{F,VS}$, which in principle may involve the interaction of any scales in the flow of size $\geq \ell$ (Aluie & Eyink 2010).

The term $\Pi_K^{F,SSA}$ describes the contribution to the TKE flux arising from the process of strain self-amplification (SSA) whereby the filtered strain-rate field $\tilde{\mathbf{s}}$ interacts with itself due to nonlinearity to either amplify (if $\tilde{\mathbf{s}} : (\tilde{\mathbf{s}} \cdot \tilde{\mathbf{s}}) < 0$) or else suppress (if $\tilde{\mathbf{s}} : (\tilde{\mathbf{s}} \cdot \tilde{\mathbf{s}}) > 0$) the strain-rate magnitude $\|\tilde{\mathbf{s}}\|$. The term $\Pi_K^{F,VS}$ describes the contribution to the TKE flux arising from the process of VS whereby the filtered strain-rate field $\tilde{\mathbf{s}}$ either amplifies

(if $\tilde{\mathbf{s}} : (\tilde{\omega}\tilde{\omega}) > 0$) or else suppresses (if $\tilde{\mathbf{s}} : (\tilde{\omega}\tilde{\omega}) < 0$) the enstrophy $\|\tilde{\omega}\|^2$ through the process of vortex stretching (or compression).

The average of the contribution from the filtered field $\Pi_K^F = \Pi_K^{F,SSA} + \Pi_K^{F,VS}$ in (2.22) is similar to the expression for the TKE flux in a two-point Kármán–Howarth equation derived using filtering and an asymptotic expansion (Carbone & Bragg 2020). Moreover, due to the relation of Betchov (Betchov 1956; Eyink 2006), $\langle \Pi_K^{F,SSA} \rangle = 3\langle \Pi_K^{F,VS} \rangle$ for incompressible homogeneous turbulence, so that the contribution of SSA to $\langle \Pi_K^F \rangle$ is three times larger than that from VS. The sub-grid contributions $\Pi_K^{SG,SSA}$ and $\Pi_K^{SG,VS}$ are similar to $\Pi_K^{F,SSA}$ and $\Pi_K^{F,VS}$ except that in the SG contributions, the filtered strain rate $\tilde{\mathbf{s}}$ acts to amplify the strain rate at sub-grid scales (for $\Pi_K^{SG,SSA}$) and vorticity at sub-grid scales (for $\Pi_K^{SG,VS}$). DNS data in Johnson (2020, 2021) showed that $\langle \Pi_K^{SG,SSA} \rangle \approx \langle \Pi_K^{SG,VS} \rangle$ in the inertial range of isotropic turbulence, so that overall, the SSA mechanism contributes more to the average energy cascade $\langle \Pi_K \rangle$ than VS does, contrary to the traditional explanation according to which VS is seen as the key mechanism driving the energy cascade (Taylor 1938; Tennekes & Lumley 1972; Davidson 2004; Doan *et al.* 2018).

The result in (2.22) also applies to SSST because it makes no assumption about the flow dynamics. As such, in SSST, SSA and VS will still be the key dynamical processes governing the TKE flux. Moreover, the relation of Betchov (1956) still applies (since it assumes only incompressibility and homogeneity; it does not assume isotropy). Therefore, at least with respect to the filtered field contribution, $\langle \Pi_K^F \rangle$, SSA still contributes three times as much as VS to the total TKE flux. The relative contribution of $\langle \Pi_K^{SG,SSA} \rangle$ and $\langle \Pi_K^{SG,VS} \rangle$ to $\langle \Pi_K^{SG} \rangle$, however, may differ from that in HIT. Moreover, the actual behaviour of the SSA and VS processes in SSST may differ appreciably from that in isotropic turbulence, since, for example, in SSST, internal waves can contribute to the behaviour of $\tilde{\mathbf{s}}$ and $\tilde{\omega}$, and anisotropy in the flow can modify the alignments between $\tilde{\mathbf{s}}$ and $\tilde{\omega}$ (see Sujovolsky & Mininni 2020) which affects the VS process. Some of these more involved questions will be the subject of a forthcoming work. A key point to be explored here is the relative contributions of Π_K^F and Π_K^{SG} to Π_K , and the correlations between these terms, which is important to understand for LES modelling of SSST.

Following the procedure outlined in Johnson (2020, 2021), a result analogous to (2.22) can be derived for Π_P :

$$\Pi_P = \Pi_P^F + \Pi_P^{SG,S} + \Pi_P^{SG,V}, \tag{2.25}$$

$$\Pi_P^F = -\ell^2 \tilde{\mathbf{s}} : (\nabla \tilde{\phi} \nabla \tilde{\phi}), \tag{2.26}$$

$$\Pi_P^{SG,S} = -\nabla \tilde{\phi} \cdot \int_0^{\ell^2} \tau_\beta (\nabla \tilde{\phi}^{\sqrt{\alpha}}, \tilde{\mathbf{s}}^{\sqrt{\alpha}}) d\alpha, \tag{2.27}$$

$$\Pi_P^{SG,V} = -\nabla \tilde{\phi} \cdot \int_0^{\ell^2} \tau_\beta (\nabla \tilde{\phi}^{\sqrt{\alpha}}, \tilde{\mathbf{r}}^{\sqrt{\alpha}}) d\alpha, \tag{2.28}$$

where $(\cdot)^{\sqrt{\alpha}}$ denotes filtering at scale $\sqrt{\alpha}$ (rather than scale ℓ), and for arbitrary first-order \mathbf{p} and second-order \mathbf{q} tensor fields, τ_β is defined as $\tau_\beta(\mathbf{p}, \mathbf{q}) \equiv \tilde{\mathbf{p}} \cdot \tilde{\mathbf{q}}^\beta - \tilde{\mathbf{p}}^\beta \cdot \tilde{\mathbf{q}}$, with $\beta \equiv \sqrt{\ell^2 - \alpha}$, and $\mathbf{r} \equiv (\nabla \mathbf{u} - [\nabla \mathbf{u}]^T)/2$ is the rotation-rate tensor. The rotational motion in the flow makes no explicit contribution to the filtered flux Π_P^F because $\tilde{\mathbf{r}} : (\nabla \tilde{\phi} \nabla \tilde{\phi}) = 0$,

although it does affect Π_p^F implicitly since rotation in the fluid affects the alignment between $\tilde{\mathbf{s}}$ and $\nabla\tilde{\phi}$.

The contribution from the filtered field Π_p^F describes the flux of TPE associated with the amplification (if $\tilde{\mathbf{s}} : (\nabla\tilde{\phi} \nabla\tilde{\phi}) < 0$) or suppression (if $\tilde{\mathbf{s}} : (\nabla\tilde{\phi} \nabla\tilde{\phi}) > 0$) of $\|\nabla\tilde{\phi}\|$ due to the filtered strain rate $\tilde{\mathbf{s}}$. The contribution Π_p^F is similar in form to $\Pi_K^{F,VS}$, in that both depend upon the strain-rate field $\tilde{\mathbf{s}}$ acting to amplify or suppress another dynamical field, rather than SSA in which the strain-rate field amplifies or suppresses itself. However, the negative sign appearing in Π_p^F but not in $\Pi_K^{F,VS}$ leads to a significant difference in how the strain rate contributes to these energy fluxes. In particular, if we define $\tilde{\lambda}_i$ and $\tilde{\mathbf{v}}_i$ as the i th ordered eigenvalues and eigenvectors of $\tilde{\mathbf{s}}$, then we may write the expressions as (see Carbone & Bragg 2020; Johnson 2021; Ballouz & Ouellette 2018) $\langle \Pi_K^{F,VS} \rangle = (1/4)\ell^2 \sum_{i=1}^3 \langle \tilde{\lambda}_i \|\tilde{\omega}\|^2 \cos^2 \theta_{\omega,i} \rangle$ and $\langle \Pi_p^F \rangle = -\ell^2 \sum_{i=1}^3 \langle \tilde{\lambda}_i \|\nabla\tilde{\phi}\|^2 \cos^2 \theta_{\nabla\phi,i} \rangle$, where $\theta_{\omega,i}$ denotes the angle between $\tilde{\omega}$ and $\tilde{\mathbf{v}}_i$, and similarly for $\theta_{\nabla\phi,i}$. In view of this, if $\langle \Pi_K^{F,VS} \rangle > 0$ so that VS contributes to the average downscale TKE flux, then $\langle \tilde{\lambda}_i \|\tilde{\omega}\|^2 \cos^2 \theta_{\omega,i} \rangle$ must be dominated by contributions from the extensional eigendirections of $\tilde{\mathbf{s}}$. In isotropic turbulence and for $\ell/\eta \rightarrow 0$, $\tilde{\omega}$ aligns preferentially with $\tilde{\mathbf{v}}_2$, but the contribution to $\sum_{i=1}^3 \langle \tilde{\lambda}_i \|\tilde{\omega}\|^2 \cos^2 \theta_{\omega,i} \rangle$ from $\tilde{\lambda}_1$ is larger than that from $\tilde{\lambda}_2$ since $\tilde{\lambda}_1$ tends to be much larger than the positive values of $\tilde{\lambda}_2$ (Tsinober 2001; Buaria, Bodenschatz & Pumir 2020). This is all the more true for ℓ/η in the inertial range, where the contribution from $\tilde{\lambda}_1$ to $\sum_{i=1}^3 \langle \tilde{\lambda}_i \|\tilde{\omega}\|^2 \cos^2 \theta_{\omega,i} \rangle$ is much larger than that from $\tilde{\lambda}_2$ (Carbone & Bragg 2020). In an analogous way, if $\langle \Pi_p^F \rangle = -\ell^2 \sum_{i=1}^3 \langle \tilde{\lambda}_i \|\nabla\tilde{\phi}\|^2 \cos^2 \theta_{\nabla\phi,i} \rangle > 0$, then $\sum_{i=1}^3 \langle \tilde{\lambda}_i \|\nabla\tilde{\phi}\|^2 \cos^2 \theta_{\nabla\phi,i} \rangle$ must be dominated by contributions from the compressive eigendirections of $\tilde{\mathbf{s}}$. Hence, while the VS contribution to the downscale TKE flux is generated by the amplification of $\tilde{\omega}$ due to the extensional straining motions in the flow, the downscale TPE flux is generated by the amplification of $\nabla\tilde{\phi}$ due to compressional straining motions in the flow. Similar behaviour was also suggested previously based on an LES model for scalar gradients in turbulence (Leonard 1997; Higgins, Parlange & Meneveau 2004).

The sub-grid TPE fluxes associated with the strain-rate field $\Pi_p^{SG,S}$ and rotation-rate field $\Pi_p^{SG,V}$ do not have simple interpretations (unlike $\Pi_K^{SG,SSA}$ and $\Pi_K^{SG,VS}$), but are related to the amplification of the scalar gradients at multiple scales. It is interesting, however, that the rotation-rate (and therefore vorticity) field makes an explicit contribution to the TPE flux through the sub-grid term $\Pi_p^{SG,V}$, even though it makes no explicit contribution to the filtered flux Π_p^F .

The discussion above highlights that the physical mechanisms governing the TKE and TPE fluxes in stratified turbulence are quite different, so that while both are positive on average (e.g. Lindborg 2006), it may not be reasonable to model them in similar ways. We will explore this further by considering the statistical correlation between Π_K and Π_p , which will provide insights into the extent to which they might be modelled using similar sub-grid closures in the context of LES.

3. Direct numerical simulations

In the next section, data from DNS will be analysed by computing various terms in (2.6) and (2.9) to understand the processes and mechanisms controlling the behaviour

Re_b	Ri	Re_s	Fr	L/η	ℓ_O/η	ℓ_C/η	L_P/η
160	0.157	25.12	0.48	126.35	43.90	10.36	155.62

Table 1. Table of parameters in DNS.

of the TKE and TPE across scales in SSST. The DNS data used are from the data set presented in Portwood *et al.* (2019) and Portwood, de Bruyn Kops & Caulfield (2022), which we summarize here. In the DNS, the unfiltered versions of (2.1) and (2.2) are solved with constant mean velocity gradient γ and mean density gradient ζ using the Fourier pseudospectral scheme described in de Bruyn Kops (2015) and Almalkie & de Bruyn Kops (2012), but with the mean-shear term handled using an integrating factor (Brucker *et al.* 2007; Chung & Matheou 2012; Sekimoto, Dong & Jiménez 2016).

In order to generate a statistically stationary flow, a method similar to that of Taylor *et al.* (2016) is adopted wherein the Richardson number of the flow is adjusted via g using a mass–spring damper control system with a target value for the total TKE $(1/2)\|\mathbf{u}\|^2$. With this method, the Richardson and Froude numbers are emergent in the flow, rather than imposed. In the absence of stratification, the TKE in a homogeneous turbulent shear flow grows with time (while the flow scales remain smaller than the domain size). With stratification, mechanisms such as spontaneous shear instabilities that form in the flow due to the layering provide for a downscale TKE flux. A statistically stationary, homogeneous, sheared, stably stratified flow therefore exists at a special equilibrium point where mechanisms generating a downscale TKE flux prevent the growth of TKE that would occur in the flow in the absence of stratification. Put another way, coupling of the fluctuating momentum to the density fields provides for additional energy dissipation mechanisms, which allows the sheared flow to attain a steady state.

The flow is well-resolved, with isotropic grid spacing and maximum wavenumber k_{max} satisfying $k_{max}\eta \approx 2$. In order to allow for the development of large anisotropic flow scales, a large domain of size $\mathcal{L}_x/\mathcal{L}_y = 2$, $\mathcal{L}_x/\mathcal{L}_z = 4$, $\mathcal{L}_x/L = 40$ was used, where \mathcal{L}_x , \mathcal{L}_y , \mathcal{L}_z are the dimensions of the domain in the x , y , z directions. In the x direction, 3072 grid points were used. Table 1 summarizes the parameters in the DNS.

Figure 2 shows snapshots of the spanwise, streamwise and vertical velocity components normalized by $\sqrt{2\mathcal{E}_K/3}$, as well as the fluctuating density field ρ' normalized by $\sqrt{\langle \rho' \rho' \rangle}$, for a two-dimensional plane in the streamwise and vertical directions. The snapshots illustrate clearly both the strong anisotropy in the flow and the inclination of the flow structures relative to the horizontal due to the mean velocity shear in the flow. That preferential orientation is, however, absent apparently for the vertical component corresponding to the direction in which the buoyancy force acts. Figure 3 shows the same quantities but for the filtered velocity and density fields, which also reveal strong anisotropy and preferential orientation of the flow structures. The difference between the fields visualized in figures 2 and 3 corresponds to the contribution from the small-scale fields.

4. Results and discussion

4.1. Mean-field behaviour

We begin by considering the behaviour of $\langle e_K \rangle$, $\langle e_P \rangle$ and the diagonal components of $\langle \boldsymbol{\tau} \rangle / 2$ (which correspond to the TKE associated with different components of \mathbf{u}) as a

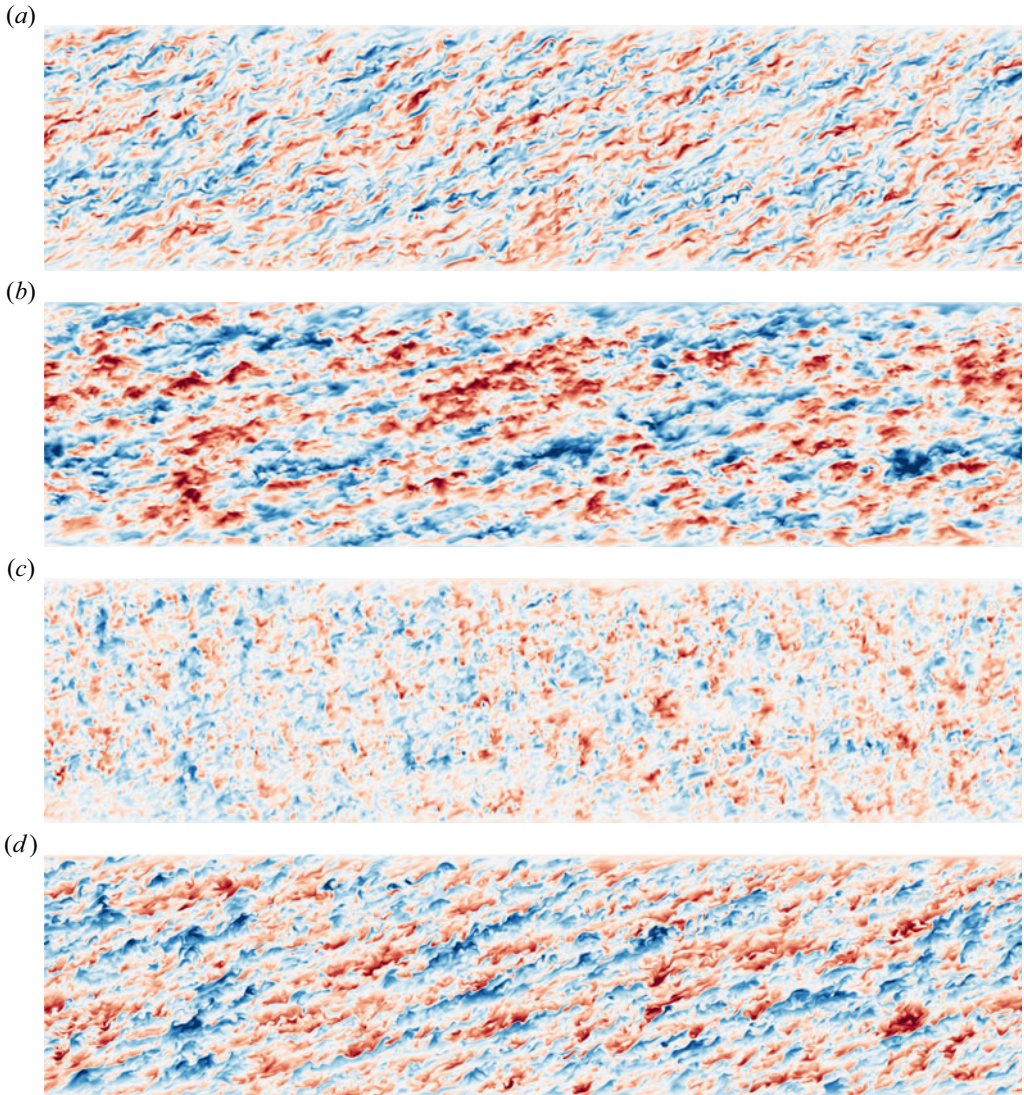


Figure 2. Snapshots of velocity and density fields from the DNS showing a plane in the streamwise and vertical directions. Normalized quantities are: (a) spanwise component $u_y/\sqrt{2\mathcal{E}_K/3}$, (b) streamwise component $u_x/\sqrt{2\mathcal{E}_K/3}$, (c) vertical component $u_z/\sqrt{2\mathcal{E}_K/3}$, (d) fluctuating density $\rho'/\sqrt{\langle\rho'\rho'\rangle}$. Values go from (red, blue), which correspond to $(-3, 3)$ for the normalized quantities, centred at white = 0. Velocities are normalized using the same scale $\sqrt{2\mathcal{E}_K/3}$ to highlight the anisotropic partitioning of kinetic energy in the flow.

function of filter length ℓ in order to understand how energy is partitioned in the flow at different scales. The results in [figure 4\(a\)](#) show that at all scales, $\langle e_K \rangle > \langle e_P \rangle$, with $\langle e_K \rangle / \langle e_P \rangle = O(10)$ at the large scales of the flow. The flow is therefore far from a state of equipartition of large-scale energy among the TKE and TPE fields, unlike the behaviour that is thought to emerge for strongly stratified flows with $Fr \ll 1$ (Billant & Chomaz 2001). Below the Corrsin scale $\ell_C = (\langle \epsilon_K \rangle / \gamma^3)^{1/2}$, the difference between $\langle e_K \rangle$ and $\langle e_P \rangle$ reduces, but remains significant even for $\ell/\eta \ll 1$. When considering the components

Analysis of scale-dependent kinetic and potential energy

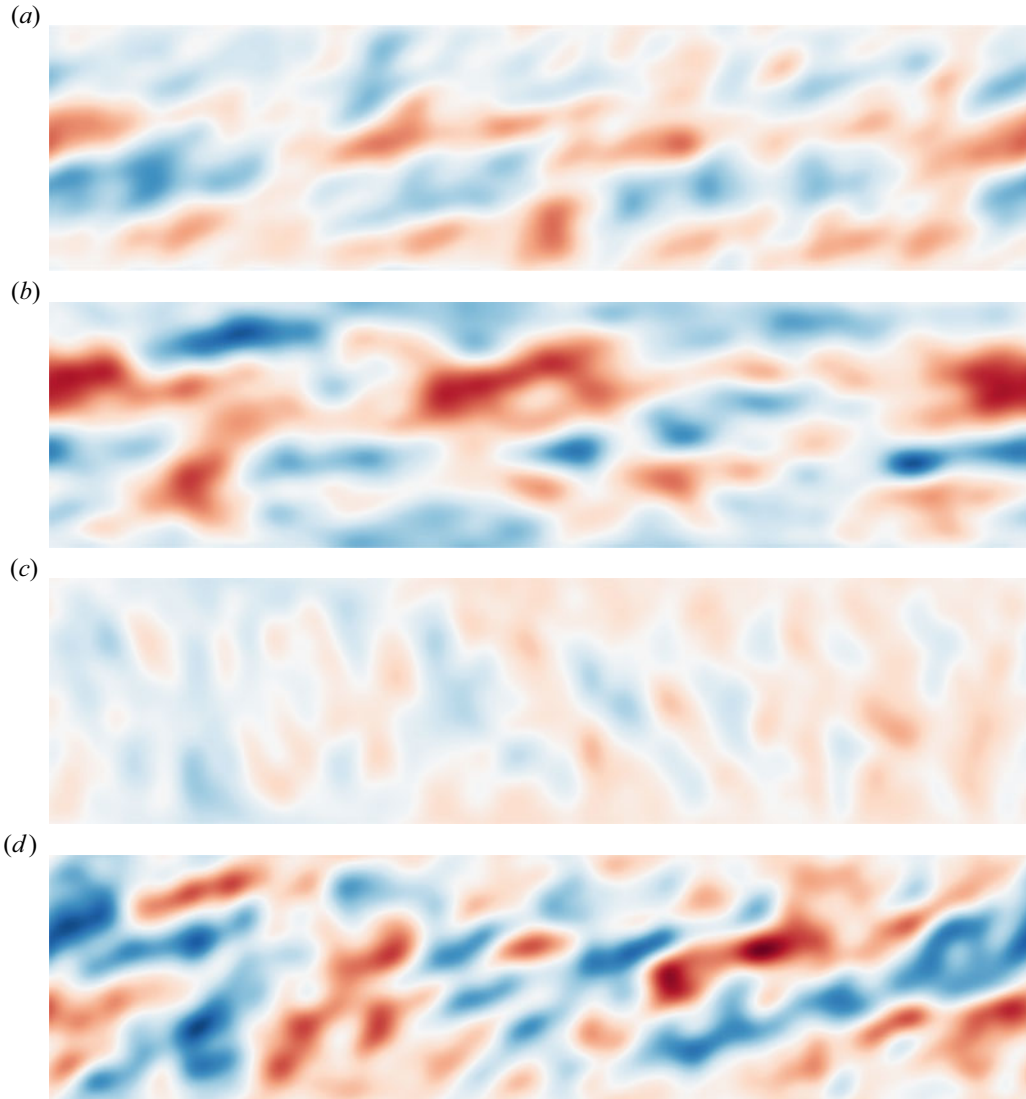


Figure 3. Snapshots of the filtered (with $\ell = 60\eta$) velocity and density fields from the DNS showing a plane in the streamwise and vertical directions. Normalized quantities are filtered: (a) spanwise component $\tilde{u}_y/\sqrt{2E_K/3}$, (b) streamwise component $\tilde{u}_x/\sqrt{2E_K/3}$, (c) vertical component $\tilde{u}_z/\sqrt{2E_K/3}$, (d) fluctuating density $\tilde{\rho}'/\sqrt{\langle \tilde{\rho}'^2 \rangle}$. Values go from (red, blue), which correspond to $(-3, 3)$ for the normalized quantities, centred at white = 0. Velocities are normalized using the same scale $\sqrt{2E_K/3}$ to highlight the anisotropic partitioning of kinetic energy in the flow.

$\langle \tau \rangle / 2$, it is seen that although the total TKE is much larger than the TPE, the TKE associated with particular components of the velocity field is comparable to the TPE. In particular, $\langle \tau_{zz} \rangle / 2 \approx 0.8 \langle e_p \rangle$ and $\langle \tau_{yy} \rangle / 2 \approx 1.3 \langle e_p \rangle$ at the large scales. As such, even though the energy contained in the TPE field is small compared to that in the total TKE field, it is of the same order as that contained in the spanwise (y) and vertical (z) directions of the flow, and therefore plays an important energetic role in the system. In terms of scaling, $\langle e_K \rangle$ and $\langle e_p \rangle$ both show the expected behaviour $\langle e_K \rangle \propto \ell^2$ and $\langle e_p \rangle \propto \ell^2$ at

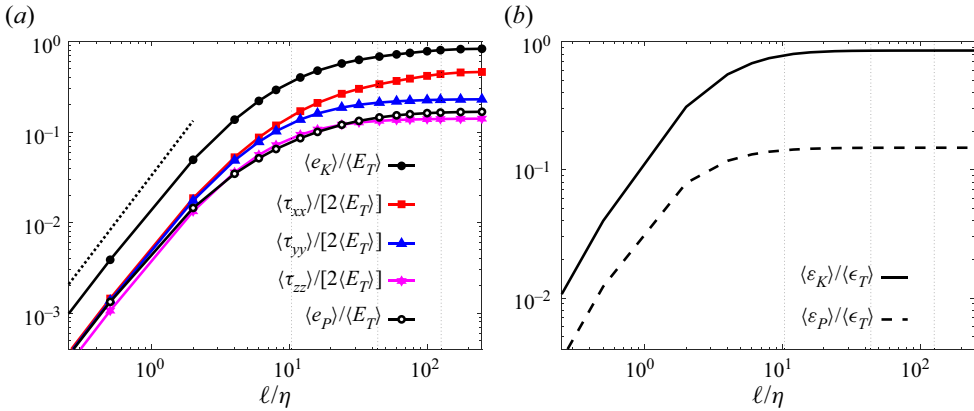


Figure 4. (a) Plot of mean small-scale TKE $\langle e_K \rangle$, TPE $\langle e_P \rangle$, and diagonal components of $\langle \tau \rangle / 2$, normalized by total energy $\langle E_T \rangle \equiv \lim_{\ell/\eta \rightarrow \infty} [\langle e_K \rangle + \langle e_P \rangle]$, as a function of filter scale ℓ . The thick dotted line indicates scaling $\propto \ell^2$. (b) Plot of mean small-scale TKE $\langle \epsilon_K \rangle$ and TPE $\langle \epsilon_P \rangle$ dissipation rates, normalized by the total turbulent energy dissipation rate $\langle \epsilon_T \rangle \equiv \lim_{\ell/\eta \rightarrow \infty} [\langle \epsilon_K \rangle + \langle \epsilon_P \rangle]$. The thin vertical dotted lines from right to left are L/η , ℓ_O/η , $\ell_C/\eta = 126.3, 43.9, 10.4$, respectively.

$\ell/\eta \leq O(1)$, where viscous effects lead to smooth velocity and density fields. Outside of this, a well-defined scaling regime does not emerge, due to the limited Reynolds number of the flow (as well as the fact that ℓ_C/η is too small for an inertially dominated regime to emerge).

In figure 4(b) we consider the mean small-scale turbulent kinetic $\langle \epsilon_K \rangle$ and potential $\langle \epsilon_P \rangle$ energy dissipation rates. For $\ell/\eta \rightarrow \infty$, these satisfy $\langle \epsilon_K \rangle \rightarrow \langle \epsilon_K \rangle$ and $\langle \epsilon_P \rangle \rightarrow \langle \epsilon_P \rangle$, and the results show that these are in the ratio $\langle \epsilon_K \rangle / \langle \epsilon_P \rangle \approx 5$. Both $\langle \epsilon_K \rangle$ and $\langle \epsilon_P \rangle$ are approximately independent of ℓ only down to $\ell/\eta = O(10)$, consistent with the usual observation that the Kolmogorov scale underestimates the scale at which viscous forces become important (Pope 2000).

We now turn to consider the contributions to the equations governing $\langle e_K \rangle$ and $\langle e_P \rangle$. The results in figure 5 show that the flow exhibits the $\ell/L \rightarrow \infty$ asymptotic behaviour $\langle \mathcal{F}_K \rangle^\infty \sim -\langle \mathcal{B} \rangle^\infty + \langle \epsilon_K \rangle$ for $\ell/\eta \gtrsim O(100)$, which corresponds to $\ell/L \gtrsim O(1)$. As ℓ/η is decreased below $O(100)$, $\langle \Pi_K \rangle$ begins to increase and becomes positive, indicating a downscale flux of TKE, as has been observed previously for stratified turbulent flows (Riley & de Bruyn Kops 2003; Lindborg 2005, 2006; Waite & Bartello 2006; Brethouwer *et al.* 2007). However, it does not become significant until $\ell/\eta \lesssim O(10)$. Moreover, when it reaches its peak value, it does not exhibit the behaviour $\langle \Pi_K \rangle / \langle \epsilon_K \rangle \sim 1$ (the maximum value obtained is $\langle \Pi_K \rangle / \langle \epsilon_K \rangle \approx 0.46$) that would be expected for non-stratified isotropic turbulence. This is because $\langle \Pi_K \rangle$ cannot grow significantly until ℓ is small enough such that $\langle \mathcal{F}_K \rangle \ll \langle \mathcal{F}_K \rangle^\infty$, which occurs only for $\ell \leq O(\ell_C)$. Once this regime is obtained, since $\ell_C < \ell_O$, the TKE balance becomes $\langle \Pi_K \rangle \sim \langle \epsilon_K \rangle$, a behaviour that can be observed in figure 5 to be approached at small scales. However, in the present flow, this behaviour does not give rise to an inertial TKE cascade since at the scales where $\langle \Pi_K \rangle \sim \langle \epsilon_K \rangle$, $\langle \epsilon_K \rangle$ is a decreasing function of ℓ . To observe an inertial TKE cascade with $\langle \Pi_K \rangle \sim \langle \epsilon_K \rangle$ would require considering a flow possessing a range of scales $\ell_O > \ell_C \gg \ell \gg \eta$. The results in figure 5 show that the contribution to the TKE flux coming from the filtered field dynamics, i.e. $\langle \Pi_K^F \rangle$, makes a significant contribution to $\langle \Pi_K \rangle$ at scales where $\langle \Pi_K \rangle$ plays a significant role in the small-scale TKE budget equation, and also that the contribution involving the

Analysis of scale-dependent kinetic and potential energy

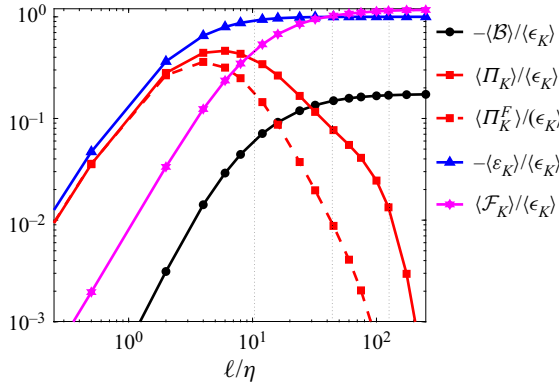


Figure 5. Plot of terms in the average small-scale TKE budget equation (2.15). Thin dotted lines from right to left are L/η , ℓ_O/η , $\ell_C/\eta = 126.3, 43.9, 10.4$, respectively.

sub-grid fields $\langle \Pi_K^{SG} \rangle$ is also significant, just as for isotropic turbulence (Johnson 2020, 2021). At sufficiently small ℓ , $\langle \Pi_K \rangle \approx \langle \Pi_K^F \rangle$, consistent with the exact limiting behaviour $\lim_{\ell/\eta \rightarrow 0} \Pi_K^F \rightarrow \Pi_K$.

The mean buoyancy term $\langle \mathcal{B} \rangle$ is negative at all scales, indicating a mean transfer of TKE to TPE, though the magnitude of $\langle \mathcal{B} \rangle$ is sub-leading compared to the other terms shown in figure 5. Nevertheless, buoyancy plays a key role in the flow because its magnitude is significant compared to the processes governing the vertical motion of the flow. As expected, the magnitude of $\langle \mathcal{B} \rangle$ begins to reduce significantly below the Ozmidov scale ℓ_O .

Concerning the TPE behaviour, the results in figure 6 exhibit the $\ell/L \rightarrow \infty$ asymptotic behaviour $\langle \mathcal{B} \rangle^\infty \sim -\langle \epsilon_P \rangle$ for $\ell/\eta \gtrsim O(100)$, which corresponds to $\ell/L \gtrsim O(1)$. The behaviour of $\langle \Pi_P \rangle$ is very similar to that of $\langle \Pi_K \rangle$ in that $\langle \Pi_P \rangle$ does not become significant until $\ell/\eta \lesssim O(10)$, and does not exhibit the behaviour $\langle \Pi_P \rangle / \langle \epsilon_P \rangle \sim 1$ (the maximum value obtained is $\langle \Pi_P \rangle / \langle \epsilon_P \rangle \approx 0.61$) that would be expected for a passive scalar advected in isotropic turbulence. Whereas the growth of $\langle \Pi_K \rangle$ is constrained in SSST to scales $\ell \leq O(\ell_C)$, as discussed previously, the growth of $\langle \Pi_P \rangle$ is constrained in SSST to scales $\ell \leq O(\ell_O)$. In our DNS, these two ranges are similar, so the ranges of scales over which $\langle \Pi_K \rangle$ and $\langle \Pi_P \rangle$ are active are similar. However, in an SSST flow with $Ri \lll 1$ and $Re \ggg 1$, this could lead to an interesting scenario where $\langle \Pi_P \rangle / \langle \epsilon_P \rangle \sim 1$ while $\langle \Pi_K \rangle / \langle \epsilon_K \rangle \approx 0$ for $\ell_O \gg \ell \gg \ell_C$. The results in figure 6 also show that like the TKE results, the contribution to the TPE flux coming from the filtered field dynamics, i.e. $\langle \Pi_P^F \rangle$, makes a significant contribution to $\langle \Pi_P \rangle$ at scales where $\langle \Pi_P \rangle$ plays a significant role in the small-scale TPE budget equation, but that the contribution involving the sub-grid fields $\langle \Pi_P^{SG} \rangle$ is also significant. At sufficiently small ℓ , $\langle \Pi_P \rangle \approx \langle \Pi_P^F \rangle$, consistent with the exact limiting behaviour $\lim_{\ell/\eta \rightarrow 0} \Pi_P^F \rightarrow \Pi_P$.

4.2. Fluctuations about the mean-field

In order to understand the energetics of the flow beyond its mean-field behaviour, we will now consider the probability density functions (PDFs) of various quantities. We begin in figures 7(a,b) with the PDFs of the normalized small-scale energies $e_K/\langle e_K \rangle$ and $e_P/\langle e_P \rangle$ for different filtering lengths ℓ/η , with the largest filter scale considered around half of

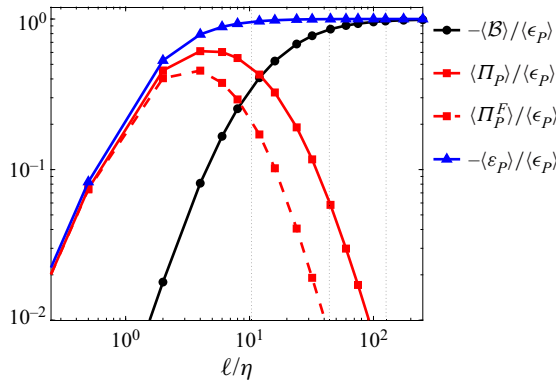


Figure 6. Plot of terms in the average small-scale TPE budget equation (2.16). Thin dotted lines from right to left are $L/\eta, \ell_o/\eta, \ell_c/\eta = 126.3, 43.9, 10.4$, respectively.

the integral length scale L . At the small scales, the PDFs are highly non-Gaussian, such that the TKE and TPE fields exhibit frequent large fluctuations about their mean-field behaviour. As the filter length increases, the heavy tails reduce, which is associated with the dominance of the linear mean-shear and buoyancy forces at the large scales of the flow, and the decreasing strength of the nonlinear term. The results also show that the TPE field exhibits stronger fluctuations from the mean-field behaviour than the TKE field (although the difference is not that large), with the difference most notable at intermediate scales. This is consistent with the fact that scalar fields are known to be more intermittent in turbulent flows because they lack the pressure gradient in their dynamics that regulates large fluctuations in the velocity gradient field.

In figure 7(c), we show the PDFs of $\Pi_K/\langle \Pi_K \rangle$ and $\Pi_P/\langle \Pi_P \rangle$ for different filtering lengths ℓ/η . At larger scales, the PDFs have a large variance, showing that at these scales, the fluxes of TKE and TPE can exceed their mean values significantly. The PDFs are also close to being symmetric, so that the probabilities of upscale and downscale fluxes of TKE are similar, and the same for TPE. As one moves to smaller scales where $\langle \Pi_K \rangle$ and $\langle \Pi_P \rangle$ both increase, the probability of large fluctuations about the mean-field behaviour reduces. However, there is still a significant probability of observing regions of the flow where the local values of Π_K and Π_P exceed significantly their mean values in magnitude. As ℓ is reduced, the mode of the PDF remains close to zero, while the mean and skewness both become positive, with the probability of downscale fluxes significantly exceeding that of upscale fluxes. The PDFs for TKE and TPE are similar in shape, and at scales where $\langle \Pi_K \rangle$ and $\langle \Pi_P \rangle$ play an important role in the TKE and TPE scalewise budgets, the fluctuations of Π_K about $\langle \Pi_K \rangle$ are larger than those of Π_P about $\langle \Pi_P \rangle$.

In figure 7(d), we show the PDFs of $\mathcal{B}/\langle \mathcal{B} \rangle$ for different filtering lengths ℓ/η . At larger scales where $-\langle \mathcal{B} \rangle$ is the dominant source term in the mean TPE budget, the fluctuations about $\langle \mathcal{B} \rangle$ are not that strong, and remarkably, the probability of observing $\mathcal{B}/\langle \mathcal{B} \rangle < 0$, which would correspond to conversion of TPE to TKE, is zero. For smaller scales, the probability of observing $\mathcal{B}/\langle \mathcal{B} \rangle < 0$ becomes finite, and increases with decreasing ℓ . The significant fluctuations of \mathcal{B} about its mean value indicate that the effects of buoyancy could be felt at scales considerably smaller than the mean-field description suggests.

The significant increase in the width of the PDFs observed in figures 7(c,d) for $\Pi_K/\langle \Pi_K \rangle$ and $\Pi_P/\langle \Pi_P \rangle$ as ℓ/η increases, and for $\mathcal{B}/\langle \mathcal{B} \rangle$ as ℓ/η decreases, is due mainly to the fact that the standard deviations of the variables are much larger than their mean

Analysis of scale-dependent kinetic and potential energy

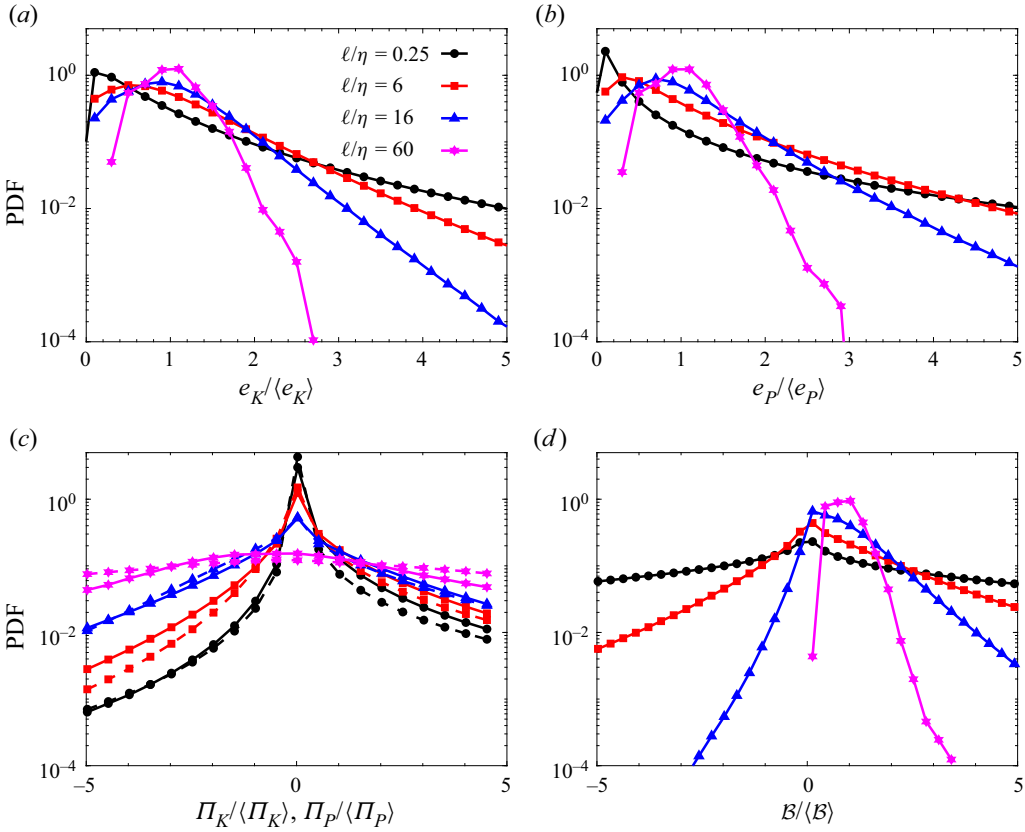


Figure 7. Plots of PDFs of (a) $e_K/\langle e_K \rangle$, (b) $e_P/\langle e_P \rangle$ and (d) $B/\langle B \rangle$ for different filter lengths ℓ . In (c), the solid lines correspond to the PDFs of $\Pi_K/\langle \Pi_K \rangle$, and the dashed lines correspond to the PDFs of $\Pi_P/\langle \Pi_P \rangle$. Different colours/symbols correspond to different ℓ/η as indicated by the legend in (a).

values in these ranges of ℓ/η . This is illustrated in figure 8 where we show the standard deviations of the variables Π_K , Π_P , $-\mathcal{B}$ normalized by their means, as functions of scale ℓ/η .

In figure 9, we show the joint PDFs of $\Pi_P/\langle \Pi_P \rangle$ and $\Pi_K/\langle \Pi_K \rangle$ for different filtering lengths ℓ/η . The results reveal that there is a very weak positive correlation between Π_P and Π_K across all scales, and the correlation is largest at $\ell/\eta = 16$. Indeed, the probability of observing a downscale TKE flux with an upscale TPE flux, and vice versa, is quite significant. This relatively weak correlation can be understood in view of the discussion in § 2.4 regarding the mechanisms governing the TKE and TPE fluxes. It is common to model TKE and TPE fluxes using similar closures but with a coefficient that accounts for their differences only through the Prandtl number effects. However, the weak correlation between Π_K and Π_P revealed in figure 9 shows that such an approach is not suitable, and that the closures need to reflect to some extent the different physical processes dominating these fluxes, which leads to the relatively weak correlation between Π_K and Π_P . In the context of LES, the contributions to Π_K and Π_P from the filtered field dynamics, namely $\Pi_K^F \equiv \Pi_K^{F,SSA} + \Pi_K^{F,VS}$ and Π_P^F (see § 2.4), are closed since they depend on only the filtered field quantities, not the sub-grid fields. It is therefore of particular interest to understand how these terms contribute to the total TKE and TPE

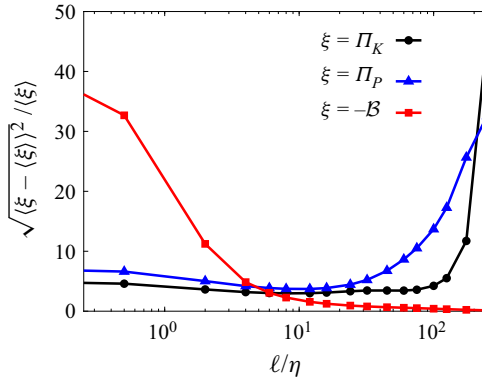


Figure 8. Plots of $\sqrt{\langle \xi - \langle \xi \rangle \rangle^2} / \langle \xi \rangle$ for $\xi = \Pi_K$, $\xi = \Pi_P$ and $\xi = -B$ as functions of filter scale ℓ/η to illustrate how the standard deviation of a variable compares to its mean value at different scales.

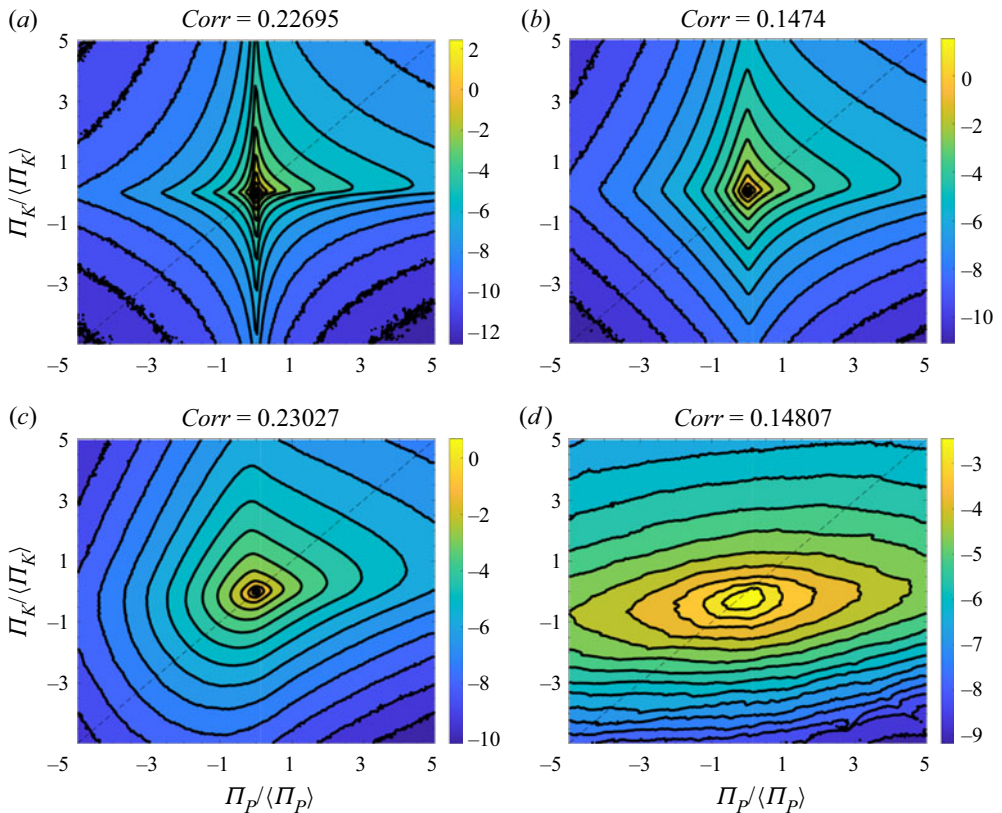


Figure 9. Contour plot of the logarithm of the joint PDF of $\Pi_P/\langle \Pi_P \rangle$ and $\Pi_K/\langle \Pi_K \rangle$ for (a) $\ell/\eta = 0.25$, (b) $\ell/\eta = 6$, (c) $\ell/\eta = 16$, (d) $\ell/\eta = 60$. Colours correspond to the logarithm of the PDF, and the correlation coefficient is shown at the top of each plot.

fluxes in the flow. To explore this, in figure 10 we consider the joint PDF of Π_K and Π_K^F for different filtering lengths ℓ/η . The filtered fluxes satisfy $\lim_{\ell/\eta \rightarrow 0} \Pi_K^F \rightarrow \Pi_K$, and the results for $\ell/\eta = 0.25$ are approaching this regime, showing a very small probability of

Analysis of scale-dependent kinetic and potential energy

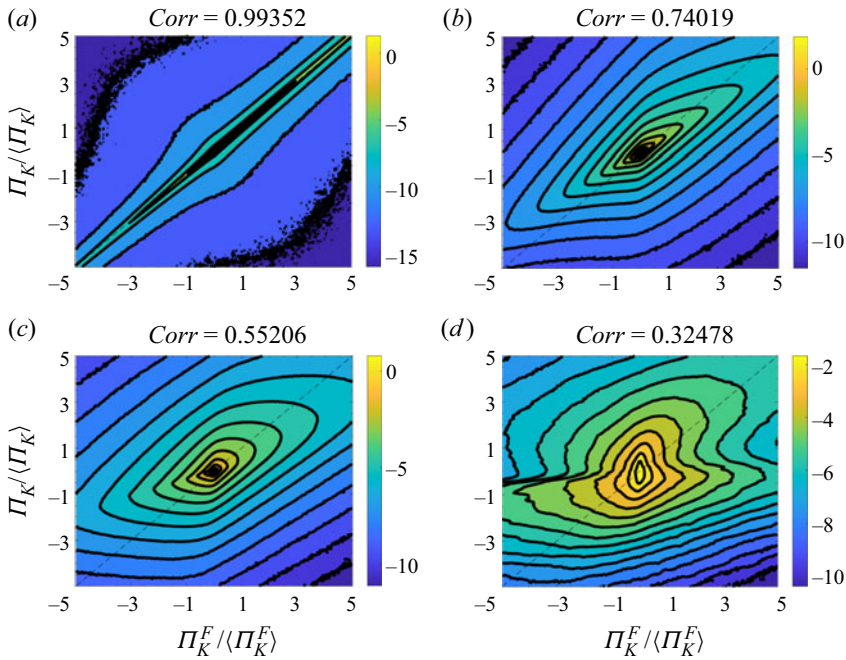


Figure 10. Contour plot of the logarithm of the joint PDF of $\Pi_K/\langle\Pi_K\rangle$ and $\Pi_K^F/\langle\Pi_K^F\rangle$ for (a) $\ell/\eta = 0.25$, (b) $\ell/\eta = 6$, (c) $\ell/\eta = 16$, (d) $\ell/\eta = 60$. Colours correspond to the logarithm of the PDF, and the correlation coefficient is shown at the top of each plot.

events deviating from the state $\Pi_K = \Pi_K^F$. As ℓ/η is increased, there remains a significant positive correlation between the variables Π_K and Π_K^F , indicating that Π_K^F makes an important contribution to the total flux Π_K , consistent with the mean-field results in figure 5. However, there is a significant probability of events where either Π_K^F and Π_K have significantly different magnitudes, or else even have opposite signs. In terms of the physical mechanisms discussed in § 2.4, this means that at a given scale ℓ , if the strain and vorticity fields are being amplified at that scale by nonlinearity such that $\Pi_K^F > 0$, this may nevertheless not lead to a downscale flux of TKE associated with $\Pi_K > 0$ since at scales smaller than ℓ , the strain and vorticity fields may be experiencing suppression (rather than amplification) due to nonlinearity yielding $\Pi_K^{SG} < 0$, and if this is strong enough, then $\Pi_K = \Pi_K^F + \Pi_K^{SG} < 0$. The spread of the PDF about the line $\Pi_K = \Pi_K^F$ also implies that the relative contribution of Π_K^F to Π_K is similar both during events where $\Pi_K \sim \langle\Pi_K\rangle$ and in large fluctuations where $|\Pi_K| \ll \langle\Pi_K\rangle$ or $|\Pi_K| \gg \langle\Pi_K\rangle$. For $\ell/\eta = 60$, the results show that Π_K and Π_K^F are almost uncorrelated, and at this scale, $\langle\Pi_K\rangle/\langle\Pi_K^F\rangle \approx 43$, so that the filtered field makes a small, uncorrelated contribution to Π_K , which is itself very small at $\ell/\eta = 60$. The results for the joint PDF of Π_P and Π_P^F are shown in figure 11. These are very similar to the TKE flux results, with $\Pi_P^F \sim \Pi_P$ observed at the smallest scales, and a significant correlation between the two at intermediate scales. The correlation between Π_P^F and Π_P is, however, slightly stronger than that between Π_K and Π_K^F .

In figure 12, we consider the joint PDF of \mathcal{B} and Π_K for different filter lengths ℓ . The results show that as ℓ is decreased, the PDF reorients from being extended along the Π_K axis, to being extended along the \mathcal{B} axis. Furthermore, the peak of the PDF (indicating the mode) is along $\Pi_K/\langle\Pi_K\rangle \approx 0$ for small scales and $\mathcal{B}/\langle\mathcal{B}\rangle > 0$ for larger scales, which

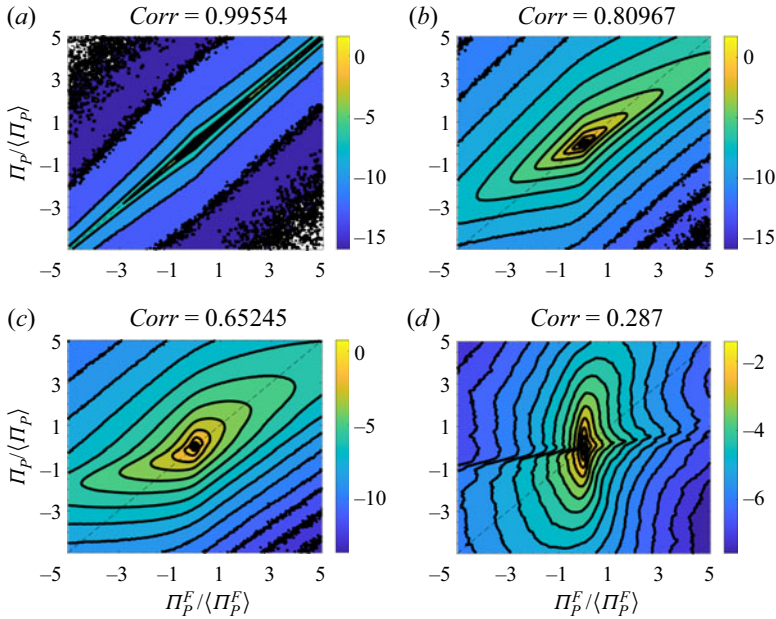


Figure 11. Contour plot of the logarithm of the joint PDF of $\Pi_P / \langle \Pi_P \rangle$ and $\Pi_P^E / \langle \Pi_P^E \rangle$ for (a) $\ell/\eta = 0.25$, (b) $\ell/\eta = 6$, (c) $\ell/\eta = 16$, (d) $\ell/\eta = 60$. Colours correspond to the logarithm of the PDF, and the correlation coefficient is shown at the top of each plot.

is associated with the different levels of skewness of these random variables at these scales. This corresponds to the transition from larger scales where buoyancy plays a more dominant role in the TKE energetics, to smaller scales where the nonlinear energy flux plays a dominant role. As also observed in figure 7(d), at larger scales the probability of observing $\mathcal{B} / \langle \mathcal{B} \rangle < 0$ is very low, suggesting that convective motion is very rare at these scales. As ℓ decreases, however, the probability of observing $\mathcal{B} / \langle \mathcal{B} \rangle < 0$ increases significantly. At $\ell/\eta = 16$, $-\langle \mathcal{B} \rangle \approx \langle \Pi_K \rangle$, and the results in figure 12 show that at this scale, convective motion $\mathcal{B} / \langle \mathcal{B} \rangle < 0$ can occur, but the PDF is strongly skewed towards stably stratified regions that have $\mathcal{B} / \langle \mathcal{B} \rangle > 0$. Moreover, for this scale the PDF is stretched significantly along the Π_K axis, showing that fluctuations of Π_K are considerably stronger than those of \mathcal{B} about their respective mean values, which are approximately equal in magnitude at this scale. The results for the joint PDF of \mathcal{B} and Π_P are similar to those for the joint PDF of \mathcal{B} and Π_K , therefore for brevity we do not show them.

Finally, given the importance of the velocity gradient dynamics for the TKE flux, in figure 13 we plot the results for the joint PDF of the filtered velocity gradient invariants $Q \equiv -\nabla \tilde{\mathbf{u}} : \nabla \tilde{\mathbf{u}}/2$ and $R \equiv -(\nabla \tilde{\mathbf{u}} \cdot \nabla \tilde{\mathbf{u}}) : \nabla \tilde{\mathbf{u}}/3$ at different filter scales ℓ/η . In Danish & Meneveau (2018), this joint PDF was considered for isotropic turbulence, and they found that the classic sheared-drop shape of the isoproability lines is preserved as ℓ/η is varied over the range considered, while other statistical characterizations of the velocity gradients also reveal behaviour that is qualitatively similar as the filter scale is increased (Tom, Carbone & Bragg 2020). For $\ell/\eta = 0.25$, the shape of the PDF in figure 13 is identical to that observed in isotropic turbulence (Meneveau 2011), with the contours extending down the right Viellefosse tail, and a strong preference for quadrants $Q > 0$, $R < 0$ and $Q < 0$, $R > 0$. However, the results in figure 13 show that at sufficiently

Analysis of scale-dependent kinetic and potential energy

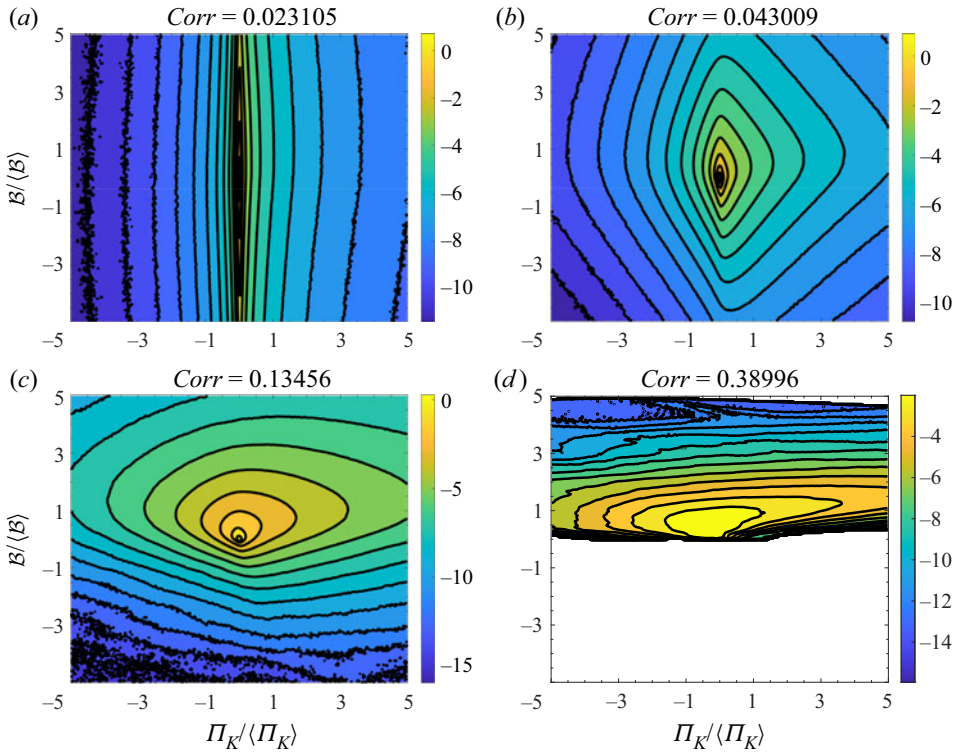


Figure 12. Contour plot of the logarithm of the joint PDF of $\mathcal{B}/\langle\mathcal{B}\rangle$ and $\Pi_K/\langle\Pi_K\rangle$ for (a) $\ell/\eta = 0.25$, (b) $\ell/\eta = 6$, (c) $\ell/\eta = 16$, (d) $\ell/\eta = 60$. Colours correspond to the logarithm of the PDF, and the correlation coefficient is shown at the top of each plot.

large scales, the shape of the PDF changes from the sheared-drop shape and becomes more symmetric. Such behaviour has also been observed for sufficiently large scales in homogeneous isotropic turbulence (Chertkov, Pumir & Shraiman 1999; Naso & Pumir 2005) and rotating turbulence (Naso & Godeferd 2012), as well as compressible turbulence (Wang *et al.* 2020). Consequently, the change in the shape of the PDF contours shown in figure 13 as ℓ/η is increased could be caused by the fact that the largest filter lengths considered are approaching large/integral scales where nonlinearity weakens, or could perhaps be due to the dominance of linear forces (e.g. buoyancy and mean-shear) at these scales.

5. Conclusions

In this paper, we have analysed the scale-dependent TKE and TPE in sheared, stably stratified turbulence (SSST) using a filtering approach, where the flow has constant mean velocity gradient and mean density gradient. Equations for the scale-dependent TKE and TPE are to explore the competing effects in the flow as well as the physical mechanisms governing the TKE and TPE fluxes between scales. Various quantities in these equations were then evaluated using data from DNS of SSST, with attention given to both the mean-field behaviour of the flow, as well as fluctuations about this mean-field state.

In terms of the mean-field properties, while the mean TKE $\langle e_K \rangle$ is larger than the mean TPE $\langle e_p \rangle$ by an order of magnitude at the large scales, the difference between

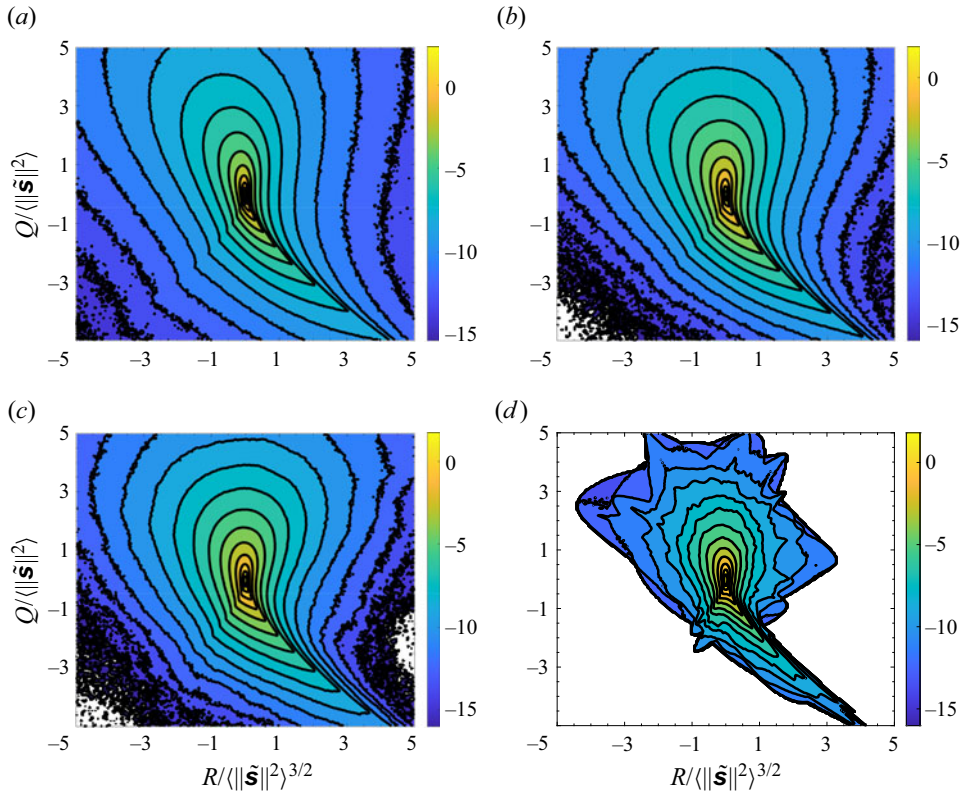


Figure 13. Contour plot of the logarithm of the joint PDF of Q and R for (a) $\ell/\eta = 0.25$, (b) $\ell/\eta = 6$, (c) $\ell/\eta = 16$, (d) $\ell/\eta = 60$. Colours correspond to the logarithm of the PDF.

them reduces with reducing scale ℓ . Nevertheless, the TPE plays an important energetic role in the system, and is larger than the vertical component of TKE at all scales in the flow. The mean small-scale TKE dissipation rate $\langle \varepsilon_K \rangle$ is also significantly larger than the potential dissipation rate $\langle \varepsilon_P \rangle$. The mean TKE and TPE fluxes between scales, $\langle \Pi_K \rangle$ and $\langle \Pi_P \rangle$, respectively, do not reveal a cascade regime in the flow due to the impact of the mean-shear down to relatively small scales in the flow. The contributions to these fluxes from the filtered fields are also shown to be significant at scales where the energy fluxes play significant roles in the energy budget equations; however, the contributions from the sub-grid fields are also important, just as has been observed for isotropic turbulence.

To understand the flow energetics beyond the mean-fields, PDFs of various quantities (normalized by their mean values) have been studied and discussed. The PDFs of small-scale TKE and TPE are highly non-Gaussian at the smallest scales, indicating large fluctuations of the TKE and TPE about their mean-field values. The TPE shows stronger fluctuations from its mean-field value than the TKE, which is consistent with the known result that scalar fields are more intermittent than velocity fields in turbulence, since scalar fields lack a pressure gradient term in their equation that can act to suppress large fluctuations. As the filter scale is increased, these PDFs approach a Gaussian distribution at scales where the linear forces in the flow (mean-shear and buoyancy) dominate the dynamics. At larger scales in the flow, buoyancy seems to convert TKE to TPE always, with

the PDF of the buoyancy term \mathcal{B} showing almost zero probability of locally convective events where $\mathcal{B} > 0$. The probability of locally convective regions increases as the filter scale is decreased, however, the probability remains small at scales downward of the Ozmidov scale. The TKE and TPE fluxes between scales are on average positive (downscale flux), with their instantaneous values correlated positively, and increasingly so with decreasing filter scale. However, the correlation is quite weak, and this is because the physical mechanisms governing the TKE and TPE fluxes are quite different, as discussed in our theoretical analysis in § 2.4. Indeed, the joint PDFs of the TKE and TPE fluxes reveal a significant probability of events where the TKE and TPE fluxes may have very different magnitudes, and even opposite signs. Finally, the PDF of the principal invariants of the filtered velocity gradients (the so-called Q, R invariants; Tsinober 2001) reveals the classical sheared-drop shape for the smallest filter scales. However, the PDF becomes increasingly symmetric about $R = 0$ as the filter scale increases. This change in shape may be caused by the fact that the largest filter lengths considered are approaching large/integral scales where nonlinearity weakens, or perhaps also due to the dominance of the linear forces associated with buoyancy and mean-shear at these scales.

This contrasts with the behaviour observed in isotropic turbulence (Danish & Meneveau 2018) and is due to the increasingly dominant effects of the linear mean-shear and buoyancy effects over the nonlinear inertial effects at these scales. This symmetry that emerges means that vortex stretching and compression become equally probable, as well as strain self-amplification and self-suppression.

One important direction for future work is to compute and explore the sub-grid scale contributions to the TKE and TPE interscale fluxes. Exploring these terms, probing in more detail the physical processes that govern them, and analysing their relation to the filtered scale flow would provide the insights required for building LES models of SSST. Work on this area will be the subject of a forthcoming article. It would also be desirable to consider a DNS of SSST flow with sufficiently large Re_b to observe a constant flux energy cascade at scales smaller than the Ozmidov and Corrsin scales, something that could not be observed in our DNS. This would enable a better assessment of the extent to which the flow at these scales is similar to the idealized case of isotropic turbulence, and the extent to which large deviations about the mean-field behaviour allow the effects of stratification to be felt even in this range. A flow with a large scale separation between the integral length and the Ozmidov scale would also allow for a better understanding of the way TKE and TPE are exchanged in this regime, and the mechanisms governing the TKE and TPE interscale fluxes in this regime, where buoyancy plays a key role. Exploring such flows is, however, very challenging computationally, and it may be some time before a flow in such a regime can be simulated with DNS.





Acknowledgements. Specifically, the Comet and Expanse clusters were used under allocation CTS170009. The DNS database was generated with funding from the US Office of Naval Research via grant N00014-15-1-2248. High performance computing resources for the DNS were provided through the US Department of Defense High Performance Computing Modernization Program by the Army Engineer Research and Development Center and the Army Research Laboratory under Frontier Project FP-CFD-FY14-007.

The contributions by G.D.P. were performed under the auspices of the US Department of Energy by Lawrence Livermore National Laboratory under contract DE-AC52-07NA27344.

Funding. A.D.B. and X.Z. acknowledge support through a National Science Foundation (NSF) CAREER award no. 2042346. This work used the Extreme Science and Engineering Discovery Environment (XSEDE), which is supported by NSF grant no. ACI-1548562 (Towns *et al.* 2014).

Declaration of interests. The authors report no conflict of interest.

Author ORCIDs.

-  Rohit Dhariwal <https://orcid.org/0000-0001-7159-7738>;
 Gavin Portwood <https://orcid.org/0000-0002-5685-4000>;
 Stephen M. de Bruyn Kops <https://orcid.org/0000-0002-7727-8786>;
 Andrew D. Bragg <https://orcid.org/0000-0001-7068-8048>.

REFERENCES

- ALAM, S., GUHA, A. & VERMA, M.K. 2019 Revisiting Bolgiano–Obukhov scaling for moderately stably stratified turbulence. *J. Fluid Mech.* **875**, 961–973.
- ALMALKIE, S. & DE BRUYN KOPS, S.M. 2012 Kinetic energy dynamics in forced, homogeneous, and axisymmetric stably stratified turbulence. *J. Turbul.* **13**, N29.
- ALUIE, H. & EYINK, G.L. 2009 Localness of energy cascade in hydrodynamic turbulence. II. Sharp spectral filter. *Phys. Fluids* **21** (11), 115108.
- ALUIE, H. & EYINK, G.L. 2010 Scale locality of magnetohydrodynamic turbulence. *Phys. Rev. Lett.* **104** (8), 081101.
- ALUIE, H. & KURIEN, S. 2011 Joint downscale fluxes of energy and potential enstrophy in rotating stratified Boussinesq flows. *Europhys. Lett.* **96** (4), 44006.
- AYET, A., KATUL, G.G., BRAGG, A.D. & REDELSPERGER, J.L. 2020 Scalewise return to isotropy in stratified boundary layer flows. *J. Geophys. Res.: Atmos.* **125** (16), e2020JD032732.
- BALLOUZ, J.G. & OUELLETTE, N.T. 2018 Tensor geometry in the turbulent cascade. *J. Fluid Mech.* **835**, 1048–1064.
- BETCHOV, R. 1956 An inequality concerning the production of vorticity in isotropic turbulence. *J. Fluid Mech.* **1**, 497–504.
- BILLANT, P. & CHOMAZ, J.-M. 2001 Self-similarity of strongly stratified inviscid flows. *Phys. Fluids* **13** (6), 1645–1651.
- BOLGIANO, R. JR. 1959 Turbulent spectra in a stably stratified atmosphere. *J. Geophys. Res. (1896–1977)* **64** (12), 2226–2229.
- BRETHOUWER, G., BILLANT, P., LINDBORG, E. & CHOMAZ, J.-M. 2007 Scaling analysis and simulation of strongly stratified turbulent flows. *J. Fluid Mech.* **585**, 343–368.
- BRUCKER, K.A., ISAZA, J.C., VAITHIANATHAN, T. & COLLINS, L.R. 2007 Efficient algorithm for simulating homogeneous turbulent shear flow without remeshing. *J. Comput. Phys.* **225**, 20–32.
- DE BRUYN KOPS, S.M. 2015 Classical turbulence scaling and intermittency in stably stratified Boussinesq turbulence. *J. Fluid Mech.* **775**, 436–463.
- BUARIA, D., BODENSCHATZ, E. & PUMIR, A. 2020 Vortex stretching and enstrophy production in high Reynolds number turbulence. *Phys. Rev. Fluids* **5**, 104602.
- CARBONE, M. & BRAGG, A.D. 2020 Is vortex stretching the main cause of the turbulent energy cascade? *J. Fluid Mech.* **883**, R2.
- CHERTKOV, M., PUMIR, A. & SHRAIMAN, B.I. 1999 Lagrangian tetrad dynamics and the phenomenology of turbulence. *Phys. Fluids* **11**, 2394–2410.
- CHUNG, D. & MATHEOU, G. 2012 Direct numerical simulation of stationary homogeneous stratified sheared turbulence. *J. Fluid Mech.* **696**, 434–467.
- DANISH, M. & MENEVEAU, C. 2018 Multiscale analysis of the invariants of the velocity gradient tensor in isotropic turbulence. *Phys. Rev. Fluids* **3**, 044604.
- DAVIDSON, P.A. 2004 *Turbulence: An Introduction for Scientists and Engineers*. Oxford University Press.
- DOAN, N.A.K., SWAMINATHAN, N., DAVIDSON, P.A. & TANAHASHI, M. 2018 Scale locality of the energy cascade using real space quantities. *Phys. Rev. Fluids* **3**, 084601.
- EYINK, G.L. 1995a Besov spaces and the multifractal hypothesis. *J. Stat. Phys.* **78** (1), 353–375.
- EYINK, G.L. 1995b Exact results on scaling exponents in the 2D enstrophy cascade. *Phys. Rev. Lett.* **74** (19), 3800.
- EYINK, G.L. 2005 Locality of turbulent cascades. *Phys. D: Nonlinear Phenom.* **207** (1–2), 91–116.
- EYINK, G.L. 2006 Cascade of circulations in fluid turbulence. *Phys. Rev. E* **74** (6), 066302.
- FERRARI, R. & WUNSCH, C. 2009 Ocean circulation kinetic energy: reservoirs, sources, and sinks. *Annu. Rev. Fluid Mech.* **41** (1), 253–282.
- GAGE, K.S. 1979 Evidence for a $k^{-5/3}$ law inertial range in mesoscale two-dimensional turbulence. *J. Atmos. Sci.* **36** (10), 1950–1954.
- GERMANO, M. 1992 Turbulence: the filtering approach. *J. Fluid Mech.* **238**, 325–336.

Analysis of scale-dependent kinetic and potential energy

- GREGG, M.C., D'ASARO, E.A., RILEY, J.J. & KUNZE, E. 2018 Mixing efficiency in the ocean. *Annu. Rev. Mar. Sci.* **10** (1), 443–473. PMID:28934598.
- HIGGINS, C.W., PARLANGE, M.B. & MENEVEAU, C. 2004 The heat flux and the temperature gradient in the lower atmosphere. *Geophys. Res. Lett.* **31** (22), L22105.
- JAYNE, S.R. 2009 The impact of abyssal mixing parameterizations in an ocean general circulation model. *J. Phys. Oceanogr.* **39** (7), 1756–1775.
- JOHNSON, P.L. 2020 Energy transfer from large to small scales in turbulence by multiscale nonlinear strain and vorticity interactions. *Phys. Rev. Lett.* **124**, 104501.
- JOHNSON, P.L. 2021 On the role of vorticity stretching and strain self-amplification in the turbulence energy cascade. *J. Fluid Mech.* **922**, A3.
- KATUL, G.G., PORPORATO, A., MANES, C. & MENEVEAU, C. 2013 Co-spectrum and mean velocity in turbulent boundary layers. *Phys. Fluids* **25** (9), 091702.
- KHANI, S. & WAITE, M.L. 2015 Large eddy simulations of stratified turbulence: the dynamic Smagorinsky model. *J. Fluid Mech.* **773**, 327–344.
- KOLMOGOROV, A.N. 1941 The local structure of turbulence in an incompressible viscous fluid for very large Reynolds numbers. *Dokl. Akad. Nauk SSSR* **30**, 299–303.
- KUMAR, A., CHATTERJEE, A.G. & VERMA, M.K. 2014 Energy spectrum of buoyancy-driven turbulence. *Phys. Rev. E* **90**, 023016.
- LEE, M.J., KIM, J. & MOIN, P. 1990 Structure of turbulence at high shear rate. *J. Fluid Mech.* **216**, 561–583.
- LEONARD, A. 1997 Large-eddy simulation of chaotic convection and beyond, p. 204. Available at: <https://arc.aiaa.org/doi/pdf/10.2514/6.1997-204>.
- LILLY, D.K. 1983 Stratified turbulence and the mesoscale variability of the atmosphere. *J. Atmos. Sci.* **40** (3), 749–761.
- LINDBORG, E. 2005 The effect of rotation on the mesoscale energy cascade in the free atmosphere. *Geophys. Res. Lett.* **32** (1), L01809.
- LINDBORG, E. 2006 The energy cascade in a strongly stratified fluid. *J. Fluid Mech.* **550**, 207–242.
- LIU, S., MENEVEAU, C. & KATZ, J. 1994 On the properties of similarity subgrid-scale models as deduced from measurements in a turbulent jet. *J. Fluid Mech.* **275**, 83–119.
- L'VOV, V. & FALKOVICH, G. 1992 Counterbalanced interaction locality of developed hydrodynamic turbulence. *Phys. Rev. A* **46**, 4762–4772.
- MENEVEAU, C. 2011 Lagrangian dynamics and models of the velocity gradient tensor in turbulent flows. *Annu. Rev. Fluid Mech.* **43** (1), 219–245.
- MENEVEAU, C. & KATZ, J. 2000 Scale-invariance and turbulence models for large-eddy simulation. *Annu. Rev. Fluid Mech.* **32** (1), 1–32.
- NASO, A. & GODEFERD, F.S. 2012 Statistics of the perceived velocity gradient tensor in a rotating turbulent flow. *New J. Phys.* **14** (12), 125002.
- NASO, A. & PUMIR, A. 2005 Scale dependence of the coarse-grained velocity derivative tensor structure in turbulence. *Phys. Rev. E* **72** (5), 056318.
- OBUKHOV, A. 1959 Effect of Archimedean forces on the structure of the temperature field in a turbulent flow. *Dokl. Akad. Nauk SSSR* **125**, 1246–1248.
- PELTIER, W.R. & CAULFIELD, C.P. 2003 Mixing efficiency in stratified shear flows. *Annu. Rev. Fluid Mech.* **35** (1), 135–167.
- POPE, S.B. 2000 *Turbulent Flows*. Cambridge University Press.
- PORTWOOD, G.D., DE BRUYN KOPS, S.M. & CAULFIELD, C.P. 2019 Asymptotic dynamics of high dynamic range stratified turbulence. *Phys. Rev. Lett.* **122**, 194504.
- PORTWOOD, G.D., DE BRUYN KOPS, S.M. & CAULFIELD, C.P. 2022 Implications of inertial subrange scaling for stably stratified mixing. *J. Fluid Mech.* **939**, A10.
- RILEY, J.J. & DE BRUYN KOPS, S.M. 2003 Dynamics of turbulence strongly influenced by buoyancy. *Phys. Fluids* **15** (7), 2047–2059.
- RILEY, J.J. & LELONG, M.-P. 2000 Fluid motions in the presence of strong stable stratification. *Annu. Rev. Fluid Mech.* **32** (1), 613–657.
- RILEY, J.J. & LINDBORG, E. 2012 *Recent Progress in Stratified Turbulence*, pp. 269–317. Cambridge University Press.
- SADEK, M. & ALUIE, H. 2018 Extracting the spectrum of a flow by spatial filtering. *Phys. Rev. Fluids* **3**, 124610.
- SEKIMOTO, A., DONG, S. & JIMÉNEZ, J. 2016 Direct numerical simulation of statistically stationary and homogeneous shear turbulence and its relation to other shear flows. *Phys. Fluids* **28** (3), 035101.
- SUJOVOLSKY, N.E. & MININNI, P.D. 2020 From waves to convection and back again: the phase space of stably stratified turbulence. *Phys. Rev. Fluids* **5**, 064802.
- TAYLOR, G.I. 1922 Diffusion by continuous movements. *Proc. Lond. Math. Soc.* **20**, 196–212.

- TAYLOR, G.I. 1938 Production and dissipation of vorticity in a turbulent fluid. *Proc. R. Soc. Lond. A Math. Phys. Sci.* **164** (916), 15–23.
- TAYLOR, J.R., DEUSEBIO, E., CAULFIELD, C.P. & KERSWELL, R.R. 2016 A new method for isolating turbulent states in transitional stratified plane Couette flow. *J. Fluid Mech.* **808**, R1.
- TENNEKES, H. & LUMLEY, J.L. 1972 *A First Course in Turbulence*. MIT Press.
- TOM, J., CARBONE, M. & BRAGG, A.D. 2020 Exploring the turbulent velocity gradients at different scales from the perspective of the strain-rate eigenframe. [arXiv:2005.04300](https://arxiv.org/abs/2005.04300).
- TOWNS, J., *et al.* 2014 Xsede: accelerating scientific discovery. *Comput. Sci. Engng* **16** (5), 62–74.
- TSINOBER, A. 2001 *An Informal Introduction to Turbulence*. Kluwer Academic Publishers.
- VALLIS, G.K. 2006 *Atmospheric and Oceanic Fluid Dynamics*. Cambridge University Press.
- VREMAN, B., GEURTS, B. & KUERTEN, H. 1994 Realizability conditions for the turbulent stress tensor in large-eddy simulation. *J. Fluid Mech.* **278**, 351–362.
- WAITE, M.L. & BARTELLO, P. 2006 The transition from geostrophic to stratified turbulence. *J. Fluid Mech.* **568**, 89–108.
- WANG, J., WAN, M., CHEN, S., XIE, C., ZHENG, Q., WANG, L.-P. & CHEN, S. 2020 Effect of flow topology on the kinetic energy flux in compressible isotropic turbulence. *J. Fluid Mech.* **883**, A11.
- WYNGAARD, J.C. 2010 *Turbulence in the Atmosphere*. Cambridge University Press.
- ZORZETTO, E., BRAGG, A.D. & KATUL, G. 2018 Extremes, intermittency, and time directionality of atmospheric turbulence at the crossover from production to inertial scales. *Phys. Rev. Fluids* **3**, 094604.